

Award Accounts

The Chemical Society of Japan Award for Young Chemists for 2008

Static and Dynamic Structures of Phenol/Ar Clusters Studied by Multiresonance Laser Spectroscopy

Shun-ichi Ishiuchi

Chemical Resources Laboratory, Tokyo Institute of Technology, 4259 Nagatsuta-cho, Midori-ku, Yokohama 226-8503

Received June 1, 2011; E-mail: ishiuchi.s.aa@m.titech.ac.jp

Static structures and dynamics of Ar atom migration in phenol/Ar clusters were investigated by using multiresonance laser spectroscopies which employ more than 3 lasers simultaneously. In the neutral ground state, phenol/Ar (1:1–4) clusters were found to adopt π-bound structure in which all Ar atoms attach to the π-cloud of benzene ring. By considering frequencies of electronic transitions of each cluster, additive rules were found, which suggest that phenol/Ar (1:2–4) clusters adopt (1|1), (3|0), and (3|1) structures, where the notation of (m|n) means that the benzene ring is wedged between m Ar atoms and n Ar atoms. On the other hand, H-bound structure, in which one Ar atom attaches to the end of an OH bond, forms in the cationic ground state generated by laser ionization of the neutral phenol/Ar clusters. According to the principle of vertical ionization, the structures just after the ionization should be π-bound structures, thus this result suggests that one Ar atom migrates from the top of a benzene ring to the end of an OH bond after the ionization. To confirm the existence of such $\pi \rightarrow$ H isomerization in cationic state, picosecond time-resolved IR spectroscopy was applied to phenol/Ar (1:2) cluster cation. By measuring the time-resolved IR spectra of OH stretching vibration, the $\pi \rightarrow$ H isomerization was successfully observed and found to be an elementary reaction with a time-constant of $\approx$7 ps. In addition, dynamic peak shift and broadening of the H-bound OH stretching band were observed and interpreted by a simple intramolecular vibrational redistribution (IVR) model.

1. Introduction

Understanding of chemical reaction mechanisms is one of the most fundamental points of chemistry. The chemical reactions of interesting large molecules have been investigated especially in condensed phase such as solution. In addition, progressive improvements in the technology of ultrafast lasers, such as femtosecond lasers, has brought significant advance to investigation of reaction mechanisms. In solution however, it is difficult to specify the number and orientation of molecules involved in the chemical reaction, therefore understanding the reaction mechanism in a clear-cut stepwise manner it is not always straightforward. Such obstacles are being overcome by several nonlinear spectroscopies,[1] however, it is difficult to specify the environment around the chemical reaction center completely. On the other hand, molecular clusters are aggregates which are composed of only molecules concerning the reaction drawn into vacuum. Because in principle the number of molecules and their orientation can be defined for each cluster, a molecular cluster can be regarded as an ideal reaction beaker. However, in traditional studies of intracluster reactions, the dynamics have been discussed on the basis of the detection of reaction products mainly by their fluorescence or mass spectrometry, which however hardly brings the advantages of the molecular clusters, i.e., observation and elucidation of chemical reaction while specifying the structures. To follow the reaction process while incorporating the structural chemistry, we developed a new method, multiresonance laser spectroscopy, in which multicolor tunable lasers are employed simultaneously. In this paper, our studies of phenol/Ar clusters by multiresonance laser spectroscopy are reviewed.

So why did we take notice of phenol/Ar clusters? Universally, intermolecular forces, such as hydrogen bonding and van der Waals forces (induced interaction and dispersion interaction), exist among molecules. These interactions are the origin of the microsolvation environment, which strongly affects biophysical and chemical phenomena, including biomolecular recognition, protein folding, biological activity, and chemical reaction mechanisms.[2] Such solvation effects are particularly important for charged species, because of the larger strength and longer range of ion–solvent interactions compared to corresponding neutral–neutral interactions.[2h,3] Biological molecules are often (locally) charged due to either (de-)protonation or charge separation. Moreover, many fundamental chemical reaction mechanisms are ion–molecule reactions, and their properties strongly depend on solvation due to large forces between the ionic species and the solvent molecules.[2g,2h] The relevance to aromatic interactions for chemical and biological recognition has been reviewed recently.[2i] The detailed understanding of these important solvation phenomena at the mo-

Published on the web October 29, 2011; doi:10.1246/bcsj.20110167

lecular level requires accurate knowledge of the intermolecular interaction potential energy surface. The phenol/Ar clusters are simple and attractive model systems to investigate the effects of stepwise solvation of Ar atoms with the charge of phenol by a well-defined number of Ar atoms.

The first published discussion of phenol/Ar clusters goes back to 1985, when Gonohe et al. reported electronic spectra obtained by resonance-enhanced multiphoton ionization (REMPI) spectroscopy and ionization potentials measured by ionization threshold spectroscopy of phenol/Ar_1 and Ar_2 (PhOH–Ar_1 and PhOH–Ar_2) clusters.[4] They found that by stepwise attachment of Ar atoms, the electronic transition energy and the ionization potential decreases at almost regular spacing. This implies that the first and second Ar atoms are surrounded by almost the same chemical environment. Thus, it was anticipated that one Ar atom sits on the benzene ring and another is on the opposite side. Hereafter, the structures in which all Ar atoms attach to the π-cloud of the benzene ring are called π-bound structure. To determine the structures of the phenol/Ar clusters, a lot of effort was made by many researchers. The analysis of electronic and vibrational transition frequencies in REMPI,[4,5] IR dip,[6] and stimulated Raman[7] spectra demonstrate that PhOH–Ar_n with $n = 1$ and 2 display π-bound structure in the neutral electronic ground and first excited state (S_0, S_1), whereby PhOH–Ar_2 was concluded to have a burger-like structure made of Ar-buns and hamburger of phenol, as mentioned above.[4] Intermolecular vibrations based on the π-bound PhOH–Ar is in agreement with high level quantum chemical calculations.[8]

The intermolecular vibrational structure in the cationic ground state (D_0) of $PhOH^+$–Ar obtained in zero-kinetic energy (ZEKE) photoelectron and mass-analyzed threshold ionization (MATI) spectra was assigned assuming a π-bound structure, and an accurate value for the dissociation energy of π-bound $PhOH^+$–Ar was derived as $535 \pm 3\,cm^{-1}$.[5b,5c,8a,9] This binding motif was further confirmed by an IR spectrum of $PhOH^+$–Ar prepared by REMPI, in which an OH stretching vibration (ν_{OH}) band was observed at $3537\,cm^{-1}$,[10] in the vicinity to the ν_{OH} band of bare $PhOH^+$ ($3534\,cm^{-1}$).[10,11] Hence, so far all spectroscopic studies have indicated that $PhOH^{(+)}$–Ar has a π-bound structure. However, the IR spectrum of $PhOH^+$–Ar generated in an electron impact (EI) ion source clearly demonstrated that H-bound structure, in which Ar attaches to the end of an OH bond, is the global minimum on the potential energy surface of the cation cluster, with a characteristic ν_{OH} frequency ($3464\,cm^{-1}$) strongly red-shifted from isolated $PhOH^+$ by H-bonding.[12] This result was confirmed by quantum chemical calculations, which predict the H-bound structure as global minimum, whereas the π-bound structure is only a local minimum.[8c,12c] Similarly, IR spectra of larger $PhOH^+$–Ar_n clusters,[12d] related $PhOH^+$–L clusters (L = He, Ne, and CH_4)[12d] as well as other acidic aromatic cations/Ar clusters[13] generated by EI demonstrated that the H-bound structure is more stable than the π-bound geometry. The reason why the most stable H-bound isomer of $PhOH^+$–Ar has completely escaped from previous spectroscopic detection (MATI, ZEKE, and REMPI-IR),[4,5b,5c,8a,9a,10] arises from the fact that the $PhOH^+$–Ar cation has been prepared by REMPI of the neutral π-bound precursor, which is governed by the restrictions of minimal geometry changes imposed by the Franck–Condon principle.

So far, we have been aware of the static structures of phenol/Ar clusters, however, the discovery of a new isomer, H-bound structure, by Dopfer and co-workers opened our eyes to the possibility of migration dynamics of Ar atom on the phenol molecule. We fortunately had a chance to collaborate with Prof. Dopfer, and started this work at 2000. At that time, we considered how we could observe the Ar migration. As mentioned above, $PhOH^+$–Ar_1 cluster generated by REMPI is (more precisely, is believed to be) π-bound structure because of the Franck–Condon principle. However, if the internal energy of $PhOH^+$–Ar_1 is increased by increasing the ionization excess energy, the Ar migration, i.e., isomerization from π-bound to H-bound structure, may occur. Furthermore, increasing the internal energy also makes a dissociation channel, i.e., $PhOH^+$–$Ar_1 \rightarrow PhOH^+ + Ar$, open. Therefore, it will be difficult to observe the Ar migration due to hiding in the dissociation. We then took notice of the $PhOH^+$–Ar_2 cluster. If the dissociation takes place together with $\pi \rightarrow H$ isomerization, the π-bound Ar atom will preferentially dissociate because binding energy of the π-bound Ar is expected to be lower than that of H-bound Ar. Therefore, if we ionize the PhOH–Ar_2 cluster with certain excess energy and measure the IR spectrum of $PhOH^+$–Ar_1 generated by dissociation of $PhOH^+$–Ar_2, the red-shifted ν_{OH}, which is a signature of the H-bound structure, may be observed. Of course, this hypothesis is on the assumption that $PhOH^+$–Ar_2 generated by REMPI with small excess energy should adopt the π-bound structure because of the vertical ionization from the π-bound neutral ground state. The IR spectrum of $PhOH^+$–Ar_2 cluster was not reported, thus we measured the IR spectrum of $PhOH^+$–Ar_2 to confirm the assumption for the first step. However, our expectation was reversed at this first experiment. The details will be mentioned later, but it was found that $PhOH^+$–Ar_2 generated by REMPI with small excess energy already adopts H-bound structure.[14] This result brought a surprise to us because the intermolecular vibrational structure of $PhOH^+$–Ar_2 produced by REMPI can be consistently explained by π-bound structure. However, our experimental results are unambiguous, so we were assured of the $\pi \rightarrow H$ isomerization at the cationic state. To clarify whether the isomerization reaction in the cation exists or not, we thought that the picosecond time-resolved multiresonance spectroscopy, which was developed to investigate excited state hydrogen transfer in phenol/ammonia clusters,[15] should give a direct answer. Then we applied the time-resolved spectroscopy to the phenol/Ar system, and successfully demonstrated the $\pi \rightarrow H$ isomerization of $PhOH^+$–Ar_2 (Figure 1).[14,16]

In this paper, I review the investigation of static structures and Ar migration dynamics of phenol/Ar clusters in accord with recent results and analyses. And as is often the case, with details becoming clear, new, and serious questions are arising. Unfortunately, I must make an admission that we have not prepared answers to these questions yet, however, it will be helpful to summarize the problems inhibiting progress of spectroscopic and dynamic investigations of phenol/Ar clusters, which are simple systems at a glance, but are quite complicated for precise analyses both from experiments and theories.

2. Experimental

Molecular clusters are produced by supersonic jet expansion, in which a mixture of vapor of solute and solvent molecules is expanded together with rare gas to vacuum through a small orifice (typical diameter is sub mm), and molecular clusters are produced by three body collision. Because of quite low concentration (10^{-10}–10^{-8} mol·l^{-1}), direct absorption spectroscopy is difficult (but not impossible[17]) under the supersonic jet conditions, however, population labeling spectroscopy,[18] in which the IR absorption, for example, is observed as change of the population of zero-vibrational level, is easier and advantageous. In this methodology, REMPI or LIF are utilized as methods to probe the population of zero-vibrational level. For that purpose, tunable UV lasers are employed. By tuning the wavelength of the UV laser to the electronic transition of the specific molecule, the population of the zero-vibrational level can be probed molecular-selectively, because the electronic transition energies are different for each species. Therefore, it is a noteworthy advantage of population labeling spectroscopy that the absorption spectrum of the specific molecule can be measured even if a number of different species (isomers) coexist.

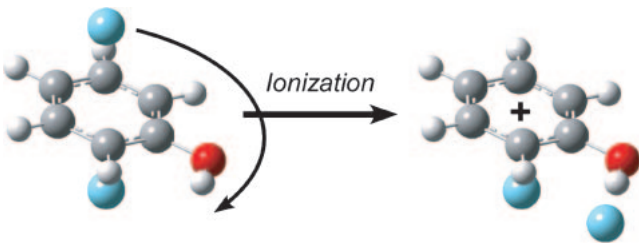

Figure 1. $\pi \rightarrow$ H isomerization in PhOH$^+$–Ar$_2$. One Ar atom of neutral π-bound structure (left) migrates to the end of OH bond (right) by photoionization of phenol.

Figure 2 shows several kinds of population labeling spectroscopies. Conventionally, the population labeling spectroscopies to measure vibrational transitions are called IR dip spectroscopy, and for measurement of electronic transitions, hole burning (HB) spectroscopy. Figure 2a shows a principle of IR dip spectroscopy in the ground (S_0) state. While monitoring the ion current of PhOH$^+$–Ar$_n$ arising from a UV laser, ν_{UV1}, which is tuned to S_1–S_0 transition of the cluster, and a second UV laser ν_{UV2}, which ionizes the electronically excited cluster by ν_{UV1}, a tunable IR laser, ν_{IR}, is fired and scanned. If ν_{IR} is resonant with a vibrational transition of the cluster, the vibrationally excited cluster dissociates and the ion current decreases. Thus, a vibrational spectrum can be measured by monitoring the depletion of the ion current (dip) as a function of ν_{IR}. If ν_{IR} is changed to a tunable UV laser ν_{UV3}, the molecular-selected electronic spectra, i.e., HB spectra, can be measured (Figure 2b). In such a measurement, also ν_{UV3} gives

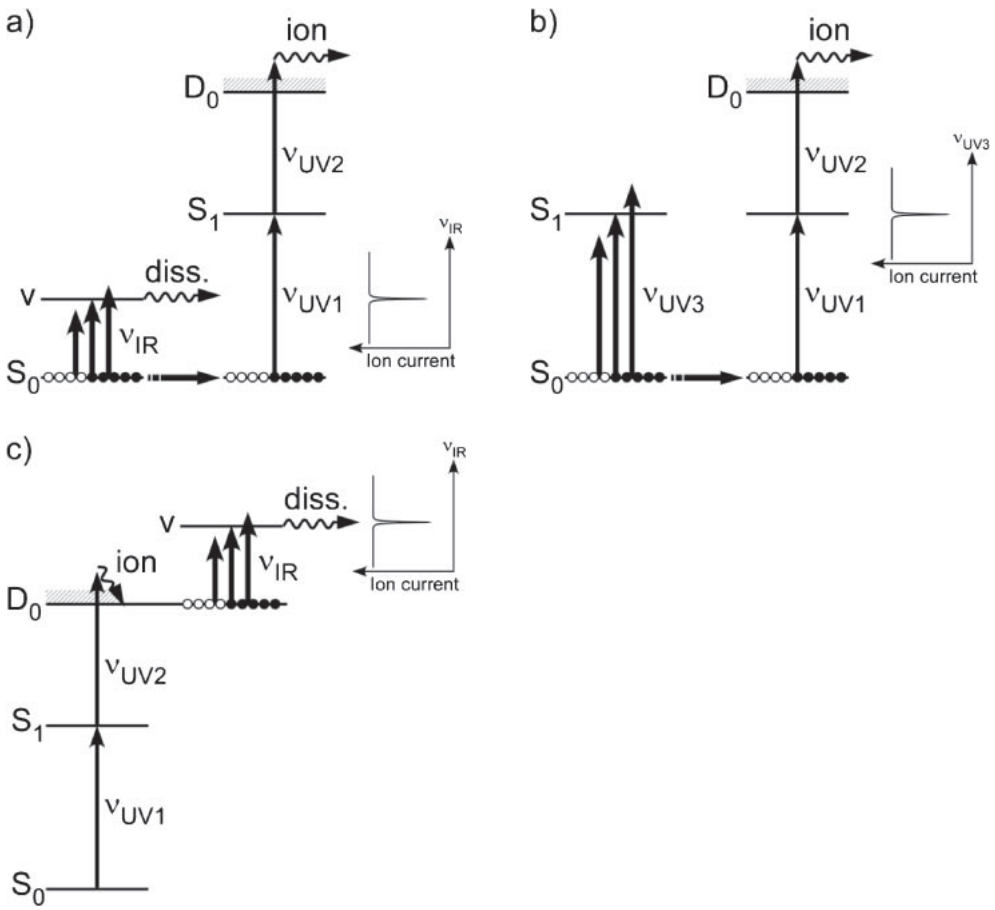

Figure 2. Schematic diagrams of several population labeling spectroscopies, a) IR dip spectroscopy in neutral ground state (S_0), b) UV–UV hole burning spectroscopy, and c) IR dip spectroscopy in cationic ground state (D_0).

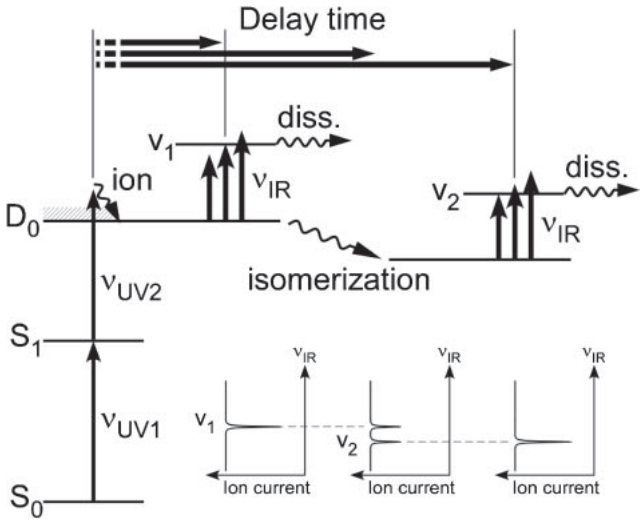

Figure 3. Principle of picosecond time-resolved IR spectroscopy. Picosecond tunable UV laser ν_{UV1} is fixed to a S_1–S_0 transition of PhOH–Ar$_n$ of specific size. Electronically excited PhOH–Ar$_n$ is ionized by another picosecond tunable UV laser ν_{UV2} which is irradiated at the same timing of ν_{UV1}. With monitoring the ion current of PhOH$^+$–Ar$_n$, picosecond tunable IR laser ν_{IR} is fired at a certain delay time after ν_{UV2} irradiation and scanned around OH stretching region. If ν_{IR} is resonant to the OH stretching vibration of π-bound (ν_1) or H-bound (ν_2) structures, the cluster dissociates and thus the ion current decreases. Therefore, by changing the delay time between ν_{UV2} and ν_{IR}, time-resolved IR spectra can be measured as depletions of the ion currents.

ion signals due to multiphoton absorption. Thus to observe the depletion of ion signal due to $\nu_{UV1} + \nu_{UV2}$, some device is necessary to avoid the ion signal due to ν_{UV3}. In this work, we applied a high voltage pulse to the deflector electrode of the mass spectrometer to eliminate the ion signal due to ν_{UV3}. On the other hand, if ν_{IR} is fired after ν_{UV2}, the IR spectra of a cationic state can be measured (Figure 2c).

If a tunable picosecond laser system is employed, the picosecond time-resolved spectroscopy can be carried out with the same methodology. Figure 3 shows the principle of picosecond time-resolved IR spectroscopy for the site switching reaction of PhOH$^+$–Ar$_n$. By changing the delay time between ν_{UV2} and ν_{IR}, the time-resolved IR spectrum at t ps after the photoionization can be measured. In principle, picosecond laser is not necessary for ν_{UV1}, however, because of convenient synchronization of the laser system, we employed a tunable picosecond UV laser for ν_{UV1} in this work.

The following laser systems were employed for the spectroscopic experiments in the nanosecond time regime, i.e., steady spectroscopy.[14,19] The UV photons, ν_{UV1} and ν_{UV2}, were obtained by frequency-doubled dye lasers (Lumonics: HD-500, Sirah: Cobra Stretch) pumped by the third and second harmonic of two Nd^{3+}:YAG lasers (Spectra Physics: GCR-170, INDI-40). Tunable IR laser radiation in the 3 μm range was generated by difference-frequency mixing using the output of a dye laser (Lumonics: HD-500/DCM) pumped by the second harmonic of a Nd^{3+}:YAG laser (Continuum: Powerlite 8100) and 532 nm radiation in $LiNbO_3$ or $KTiOAsO_4$ (KTA) crystals. The UV lasers were operated at a repetition rate of 20 Hz, whereas the IR laser was triggered at 10 Hz. Using a beam combiner, ν_{UV1} and ν_{UV2} were aligned coaxially. Both beams were focused into the molecular beam by a fused silica lens with 300 mm focal length. The counterpropagating ν_{IR} beam was focused by a CaF_2 lens with 300 mm focal length. As the lifetime of the PhOH–Ar$_n$ clusters is of the order of a few ns,[20] ν_{UV1} and ν_{UV2} were fired simultaneously.

On the other hand, the picosecond laser apparatus was as follows and is schematically shown in Figure 4.[14,15c,16] A femtosecond mode-locked Ti:sapphire laser ($\lambda = 800$ nm) pumped by the second harmonic of a Nd^{3+}:YVO_4 laser (Spectra Physics: Millennia Vs) was regeneratively amplified at 10 Hz and stretched to 3 ps (Spectra Physics, TSA 25/PRO-230). The typical pulse energy of the amplified picosecond pulse was 11–12 mJ at 800 nm. Forty percent of this pulse was frequency-doubled and used to pump two optical parametric generator/amplifiers (Light Conversion: TOPAS-400, OPA1 and OPA2). The signal outputs of OPA1 and OPA2 were frequency-doubled to generate ν_{UV1} and ν_{UV2}. A third OPA3 (Light Conversion: TOPAS-800) was pumped by 20% of the 800 nm pulse from the regenerative amplifier. The frequency-doubled idler output of this third OPA and the remaining 40% of the 800 nm light from the regenerative amplifier were differentially mixed in a KTA crystal to generate tunable IR laser light in the 3 μm range, ν_{IR}. The IR pulse energy was about 100 μJ/pulse. The pulse width of both the UV and the IR lasers of about 3 ps corresponds to the effective time resolution of the spectroscopic approach. The timing of each UV laser was independently adjusted with respect to the IR laser by two optical delay lines, which were controlled by a personal computer. Their three lasers were combined coaxially by two dichroic mirrors and focused by a 250 mm focal length CaF_2 lens into the molecular beam.

The PhOH–Ar$_n$ clusters were produced in a supersonic molecular beam by expanding a heated phenol sample (40 °C) seeded in Ar carrier gas (5 bar) through a pulsed valve (General Valve, series 9, 0.8 mm diameter) into a vacuum chamber (10^{-4} Pa). For efficient generation of the phenol/Ar clusters, it is quite important to remove water from the phenol crystal, because the cluster formation between phenol and water inhibits the generation of phenol/Ar clusters. To eliminate water, crystalline phenol is purified by vacuum sublimation and dried under vacuum prior to the experiments. In addition, a bit of heating, as mentioned above, is effective to reduce the formation of phenol/water clusters. The supersonic expansion was trimmed to a molecular beam by a skimmer, whose diameter was 2 mm. To the molecular beam, several lasers were irradiated. The ions generated by $\nu_{UV1} + \nu_{UV2}$ were extracted in a time-of-flight mass spectrometer through a deflector electrode which also behaves as a mass gate for the HB spectroscopy, and detected via a homemade Even-cup dynode convertor detector.[21] The ion signal, amplified by a preamplifier (NF: BX-31A) and analog–digital converted by a fast digitizer PCI board (Acqiris: AP240), was integrated and recorded on a personal computer as a function of scanning laser frequency.

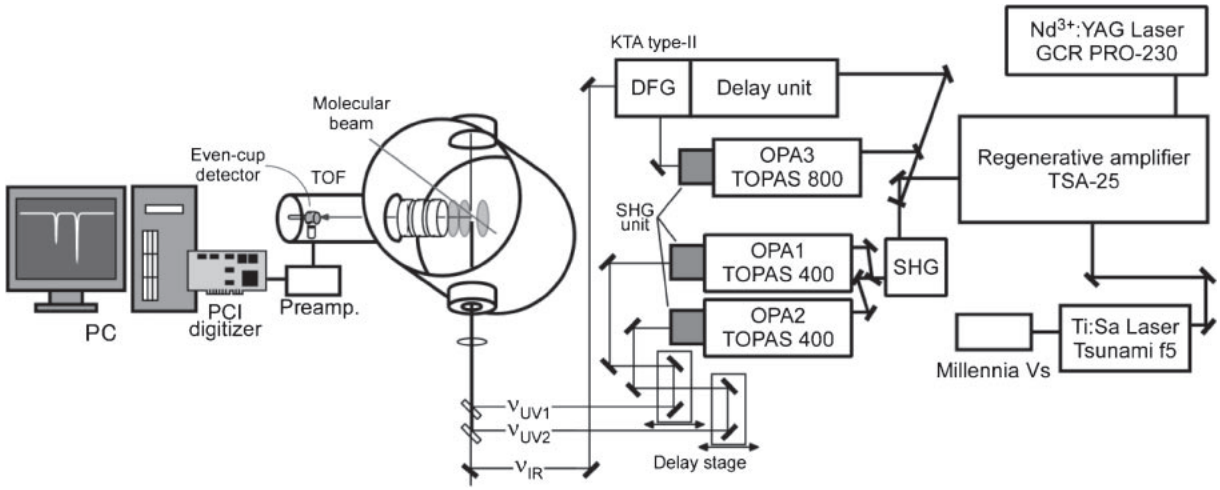

Figure 4. Schematic diagram of picosecond laser system. The second harmonic of a Nd^{3+}:YVO_4 laser (Spectra Physics: Millennia Vs) pumps a femtosecond mode-locked Ti:sapphire laser (Spectra Physics: Tsunami f5). Output of the femtosecond pulse is introduced to a regenerative amplifier (Spectra Physics: TSA-25) pumped by a 10 Hz nanosecond Nd^{3+}:YAG laser (Spectra Physics: GCR PRO-230). The regeneratively amplified pulse (3 ps, 11–12 mJ/pulse at 800 nm) is divided to three beams at an intensity ratio of 40:40:20%. The first 40% pulse is frequency-doubled and pumps two optical parametric generator/amplifiers (Light Conversion: TOPAS-400, OPA1 and OPA2). The signal outputs of OPA1 and OPA2 are frequency-doubled and used as ν_{UV1} and ν_{UV2}. The second 40% pulse and frequency-doubled idler output of a third OPA3 (Light Conversion: TOPAS-800) pumped by 20% pulse are differentially mixed in a KTA crystal (type-II phase matching condition) and converted to a tunable IR laser light in the 3 μm range, ν_{IR}. The timings of ν_{UV1} and ν_{UV2} are independently adjusted with respect to ν_{IR} by two optical delay lines. These three lasers are combined coaxially by two dichroic mirrors and focused by a CaF_2 lens with 250 mm focal length into the molecular beam. Generated ions are introduced to a homemade time-of-flight (TOF) mass spectrometer by some electrodes and detected by a homemade Even-cup detector. Ion signal is amplified by a preamplifier and recorded by a PCI digitizer board installed to a personal computer.

3. Results and Discussion

3.1 Resonance-Enhanced Multiphoton Ionization Spectra. Prior to the measurement of the IR dip spectra, S_1–S_0 transition energies of PhOH–Ar_n clusters must be known, which is necessary for determining the wavelength of ν_{UV1}. To obtain the S_1–S_0 electronic spectra, we applied resonance-enhanced multiphoton ionization (REMPI) spectroscopy to PhOH–Ar_n ($n = 1$–4) clusters, which have already been reported[4,5c,22] and their spectra were reproduced well in this work (Figure 5). These spectra were obtained by fixing the ionization UV laser, ν_{UV2}, to 310 nm (32258 cm^{-1}), and scanning the excitation UV laser, ν_{UV1}. In the figure, a REMPI spectrum of phenol monomer is also shown for comparison, which is measured by one-color REMPI, i.e., the excitation laser ν_{UV1} also performs as the ionization laser. In each spectrum of PhOH–Ar_n ($n = 1$–4) clusters, intense bands are observed at 36316, 36281, 36373, and 36338 cm^{-1}, which can be assigned to transitions from zero vibrational level of S_0 state to that of S_1 state, i.e., 0–0 transition. The 0–0 transition energy of phenol monomer is 36350 cm^{-1}, thus, their transition energies indicate shifts of −34, −69, +23, and −12 cm^{-1} from phenol monomer, respectively. Here, it is very curious that additive red shift of about 35 cm^{-1} is observed between $n = 0$–1, 1–2, and 3–4, however, a large blue shift, +92 cm^{-1}, between only $n = 2$–3. From the additive red shift between $n = 0$–1 and 1–2, Gonohe et al. concluded that the chemical environment of where Ar attaches to the bare phenol and that of where one more Ar atom attaches to PhOH–Ar_1 cluster

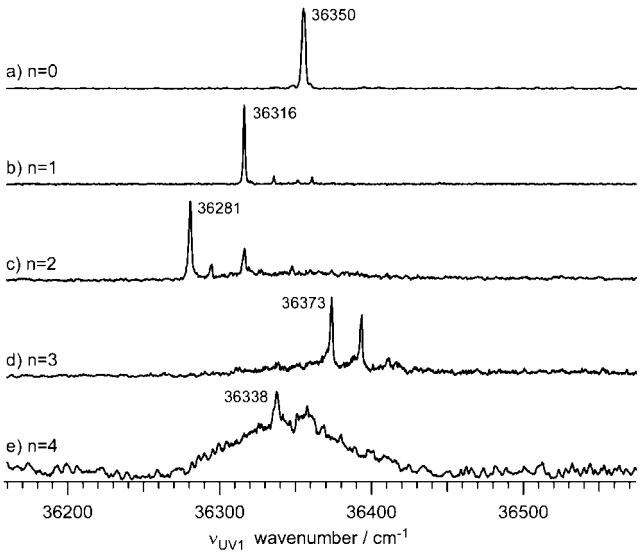

Figure 5. REMPI spectra measured by monitoring mass peaks of a) phenol monomer and b)–e) $PhOH^+$–Ar_n ($n = 1$–4).

should be almost the same, which means that Ar attaches on the benzene ring in PhOH–Ar_1 clusters, and one more Ar atom attaches on the opposite side of the benzene ring.[4] In this paper, we represent each structure as (1|0) and (1|1), respectively. This interpretation is supported by recent high-resolution spectroscopy.[22b] On the other hand, the blue shift observed in $n = 3$

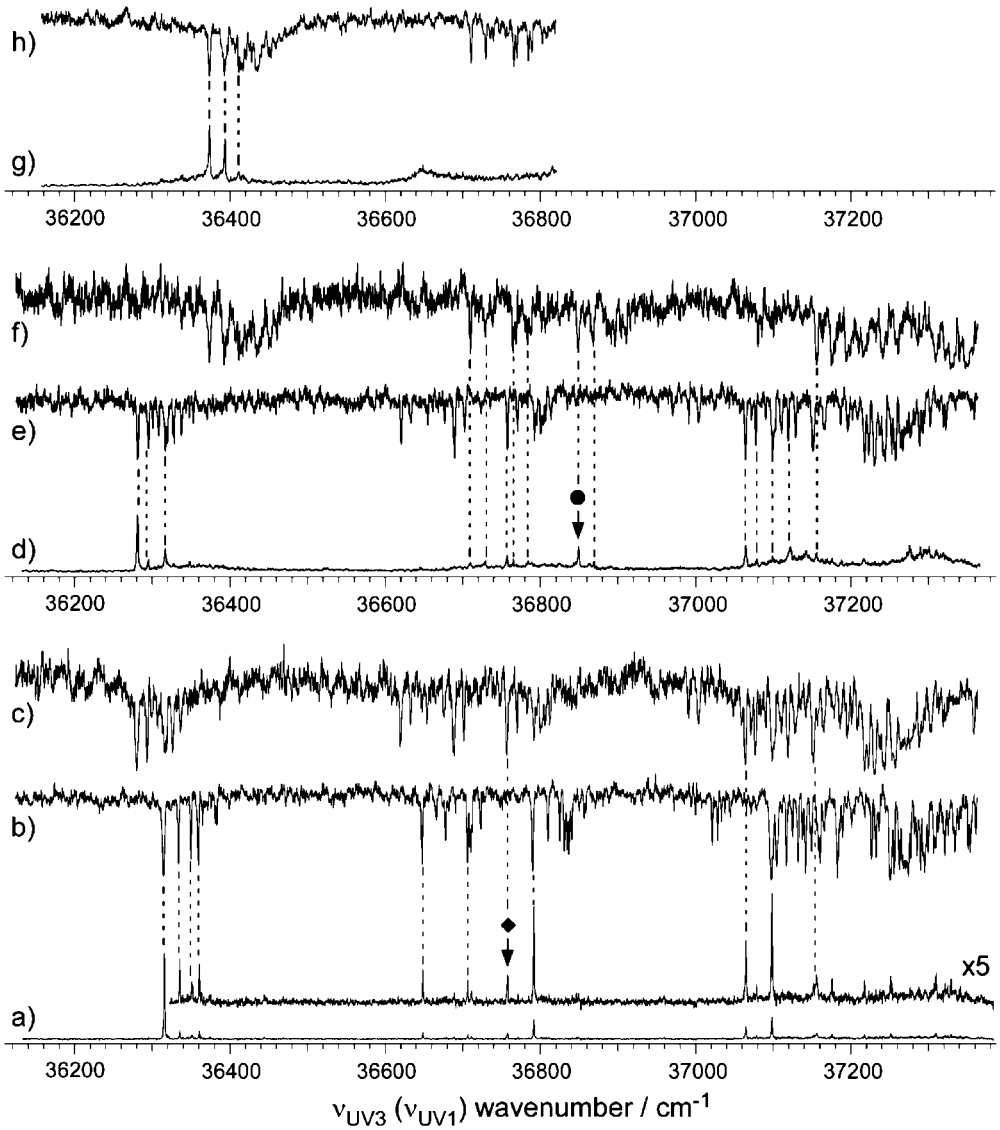

Figure 6. REMPI (a: $n = 1$, d: $n = 2$, g: $n = 3$) and HB spectra (b, c: $n = 1$, e, f: $n = 2$, h: $n = 3$) of PhOH–Ar$_n$. The HB spectrum b) was measured by fixing ν_{UV1} (Figure 2b) to 0–0 transition of PhOH–Ar$_1$ (36326 cm^{-1}). Almost every peak observed in the REMPI spectrum a) appears in the HB spectrum b) except some bands, one of which is indicated by ◆. The HB spectrum c) measured by fixing ν_{UV1} to ◆ corresponds to the HB spectrum measured by fixing ν_{UV1} to 0–0 transition of PhOH–Ar$_2$ (36281 cm^{-1}). Also in $n = 2$, almost every peak observed in the REMPI spectrum d) appears in the HB spectrum e) except some bands. By monitoring the most intense band of their bands indicated by ●, the HB spectrum f) was measured and found to correspond to the HB spectrum h) measured by fixing ν_{UV1} to 0–0 transition of PhOH–Ar$_3$ (36373 cm^{-1}).

cluster is interpreted as an indicator of (3|0) structure, in which all 3 Ar atoms attach on the same side of a benzene ring, on the basis of the structure of aniline/Ar clusters and observed binding energy of Ar atoms in PhOH–Ar$_3$.[23] From this point of view, $n = 4$ cluster should adopt (3|1) structure, because the additive red shift is observed between $n = 3$–4, which probably indicates that one Ar atom attaches on the bare benzene ring surface like $n = 0$–1 and 1–2. From these structural assignments, we can establish a simple additivity rule to predict the S_1–S_0 transition energies of any structural PhOH–Ar$_n$ cluster, which will be discussed in Section **3.3**.

3.2 Hole Burning Spectra. In the previous section, the structures of species giving the most intense electronic transition were discussed. However, there is a possibility that other isomers coexist. So, to confirm whether other isomers coexist or not, we applied hole burning (HB) spectroscopy to PhOH–Ar$_n$ ($n = 1$–3) clusters.[19b]

Figure 6a shows the REMPI spectrum of the PhOH–Ar$_1$, which is a long range version for comparison. The ionization laser, ν_{UV2}, was fixed to 310 nm (32258 cm^{-1}). The same REMPI spectrum is also reproduced with 5 times magnification along the vertical axis to show weak low-frequency bands. Figure 6b displays the HB spectrum recorded for $\nu_{UV1} =$ 36316 cm^{-1}. Because of the intense burn laser, ν_{UV3}, we successfully observed many weak bands not observed in the REMPI spectrum. By comparing these spectra, it was found that almost all of the bands observed in the REMPI spectrum appear in the HB spectrum, except for bands at 36758, 37066,

and 37156 cm^{-1}. The HB spectrum measured by fixing ν_{UV1} to 36758 cm^{-1} (indicated by ◆), is shown in Figure 6c. At a glance, it can be found that the two HB spectra shown in Figures 6b and 6c are completely different. Thus, it is concluded that the electronic transition observed at 36758 cm^{-1} derives from other species. The bands at 37066 and 37156 cm^{-1} were also observed in the HB spectrum in Figure 6c. This observation implies that the electronic transitions at 36758, 37066, and 37156 cm^{-1} originate from the same species. Thus, we observed predominantly two different species in the REMPI spectrum in Figure 6a by monitoring the $PhOH^+$–Ar_1 mass channel.

In the region below 36758 cm^{-1}, the new species shows several intense bands comparable to the bands at 36758 or 37066 cm^{-1} in the HB spectrum. However, these bands do not appear in the REMPI spectrum at all. In addition, a band observed at 36281 cm^{-1} in the HB spectrum, which seems to be a 0–0 transition of the new species, coincides with the 0–0 transition of PhOH–Ar_2. According to these results, it is a natural interpretation that the new species observed in the HB spectrum in Figure 6c is not a second isomer of the PhOH–Ar_1, but PhOH–Ar_1 cluster produced by evaporation of one Ar atom from the PhOH–Ar_2.

This interpretation is confirmed by measuring the HB spectrum of the PhOH–Ar_2 (Figure 6e). Also, the REMPI spectrum of the PhOH–Ar_2 is shown in Figure 6d. For the HB spectrum in Figure 6e, ν_{UV1} was fixed to the 0–0 transition of PhOH–Ar_2 (36281 cm^{-1}), whereas ν_{UV2} was fixed to 32258 cm^{-1}. By comparing the two HB spectra in Figures 6c and 6e, it is easily found that both spectra are the same. Thus, the bands observed at 36316, 37066, and 37156 cm^{-1} in the REMPI spectrum of PhOH–Ar_1 derive not from an isomer of PhOH–Ar_1, such as the H-bound isomer, but from Ar fragmentation of the PhOH–Ar_2. Therefore, it is concluded that the PhOH–Ar_1 cluster occurs as a single isomer in the molecular beam expansion.

Similarly to PhOH–Ar_1, we examined the existence of isomers for the PhOH–Ar_2 by comparing the REMPI spectrum of PhOH–Ar_2 (Figure 6d) with the HB spectrum (Figure 6e). At a glance, the bands observed in the REMPI spectrum also appear in the HB spectrum, except for those at 36710, 36729, 36765, 36784, 36850, 36869, and 37156 cm^{-1}. Thus, the species that give rise to these electronic transitions are different species from the probed one. However, these bands may be derived from the dissociation of larger clusters similarly to PhOH–Ar_1, so, we measured the HB spectrum by fixing ν_{UV1} to 36850 cm^{-1}, represented by ●. In the observed HB spectrum (Figure 6f), the other bands mentioned above were also observed, that is, these bands originate from the same species. The bands detected below 36710 cm^{-1} in the HB spectrum did not appear in the REMPI spectrum. Furthermore, the transition observed at 36373 cm^{-1} in the HB spectrum coincides with the 0–0 transition of the PhOH–Ar_3. Thus, this observation suggests that the carrier of this transition can also be expected to be generated by the evaporation of one Ar atom from PhOH–Ar_3. Figures 6g and 6h show the REMPI spectrum of PhOH–Ar_3 and the HB spectrum obtained by fixing ν_1 to the 0–0 band of PhOH–Ar_3, respectively. From these spectra, it is concluded that the sharp bands observed at 36710, 36729, 36765, 36784, 36850, 36869, and 37156 cm^{-1} in the REMPI spectrum in Figure 6d can be assigned to the electronic transitions of the PhOH–Ar_3 cluster, which contaminates the spectrum of PhOH–Ar_2 due to the evaporation of one Ar atom.

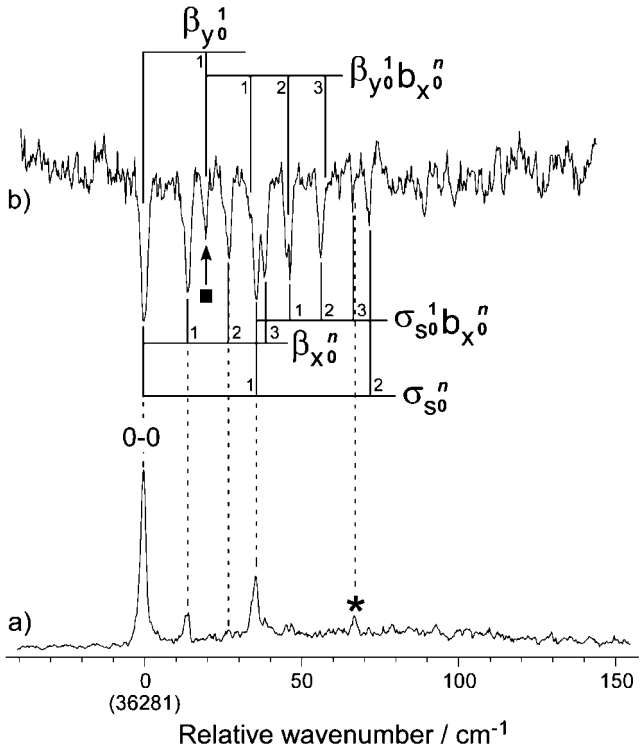

Figure 7. Comparison of a) REMPI and b) HB spectra of PhOH–Ar_2. A band indicated by * in the REMPI spectrum a) is not observed in the HB spectrum b). A band marked by ■ in the HB spectrum b) is newly observed intermolecular vibronic band.

However, by comparing REMPI and HB spectra of PhOH–Ar_2 delicately, it was found that a tiny band observed at 36348 cm^{-1} (0–0 + 67 cm^{-1}) in the REMPI spectrum does not correspond to the band observed in the HB spectrum. Figure 7 shows REMPI and HB spectra of the S_1 origin region of PhOH–Ar_2. The controversial band is marked with an asterisk. The corresponding band in the HB spectrum is slightly red-shifted. Of course, this tiny disagreement cannot be denied to be resulting from an experimental error. However, if the slightly red-shifted band observed in the HB spectrum is the same transition with the *-band, it is too weak, because two bands observed at 0–0 + 45–50 cm^{-1} are slightly weaker than the *-band in the REMPI spectrum, though the former show stronger bands in the HB spectrum than the latter. In addition, the relative intensity of this transition at 36348 cm^{-1} seems to vary substantially in the REMPI spectra recorded in different studies,[5c,5e,19b,22a,22b] which supports that this band arises from a different isomer, because the formation of different isomers strongly depends on conditions of the supersonic jet expansion as was shown in detail previously for aniline–Ar_n.[23b,24] Unfortunately, an HB spectrum monitoring this band has not been successfully observed because of the small intensity, however we tentatively assigned this band to another isomer, whose structure will be discussed in the next section.

Similarly, if the REMPI spectrum of PhOH–Ar_3 is checked carefully, one can find quite tiny bands at 36313 and 36338 cm^{-1}, which are respectively indicated by † and ‡ in Figure 8a and are not observed in the HB spectrum of Figure 8b. The frequency of the ‡-band corresponds to that of 0–0 transition of a predominant conformer of PhOH–Ar_4, thus it is presumably derived from dissociation of $PhOH^+$–Ar_4 generated via its 0–0 transition. On the other hand, for the †-band, such corresponding band is not observed, thus it is possibly assigned to a 0–0 transition of other minor isomer of PhOH–Ar_3. Structures of the minor isomers of PhOH–Ar_2 and PhOH–Ar_3 will be discussed in the next section based on additive rules of S_1–S_0 transition energies.

The advantage of the HB spectroscopy is, of course, to discriminate electronic transitions of different isomers, but another advantage is that very weak transitions which cannot be observed by REMPI spectroscopy can be clearly observed in HB spectra. In Figure 7, many peaks which are not observed in the REMPI spectrum are observed in the HB spectrum. These bands are assigned to intermolecular vibrations of PhOH–Ar_2 clusters. The assignments of the intermolecular vibrations observed in REMPI spectrum have been already reported by Schmidt et al.,[5e] which are presented in Figure 7a. The vibrational motions of the six possible intermolecular modes of the (1|1) and (2|0) structures are depicted in Figure 9. Here, the in-phase and out-of-phase sliding modes along the x axis and the y axis are represented by β_x, β_y and λ_x, λ_y, respectively. The in-phase and out-of-phase intermolecular stretching modes are represented by σ_s and σ_a, respectively. The symmetry of each mode in the C_s point group is also indicated in the figure together with the symmetry correlated with the C_{2v} point group (in parentheses). In previous assignments, the symmetry of the normal modes of the (1|1) structure was evaluated in the C_{2v} point group; that is, the OH group was regarded as an atom. This assumption was used to explain why only progressions involving two intermolecular modes are observed. In the C_{2v} point group, only two intermolecular vibrational modes (σ_s and β_x) are totally symmetric (a_1) and can be observed without vibronic coupling. On the other hand, because the proper C_s point group has three totally symmetric a′ modes (σ_s, β_x, and β_y), the (1|1) structure could display three intense vibrational modes in the electronically allowed S_1–S_0 transition. Since the (2|0) structure belongs to the C_1 point group, all the intermolecular vibrations are allowed for this isomer. Schmidt et al. argued that the appearance of two intermolecular vibrational modes in the REMPI spectrum is indicative of C_{2v} symmetry and assigned the intermolecular modes as σ_s and β_x based on a consideration of the respective reduced masses. They interpreted that Ar atoms do not feel the existence of OH hydrogen atoms. On the basis of their assignments, we assigned the vibronic bands observed in the HB spectrum. As shown in Figure 7b, almost all of the bands in the HB spectrum can be assigned by progressions and combinations of σ_s and β_x, except for a band at $0° + 20\,cm^{-1}$ represented by ■, which is not observed in the REMPI spectrum. As mentioned above, β_y is forbidden in the C_{2v} approximation, but is allowed in C_s symmetry. Therefore, the transition strength for β_y is expected to be weaker than those of σ_s and β_x. Thus, we assign the band at $0° + 20\,cm^{-1}$ to β_y.[1] This mode occurs also in

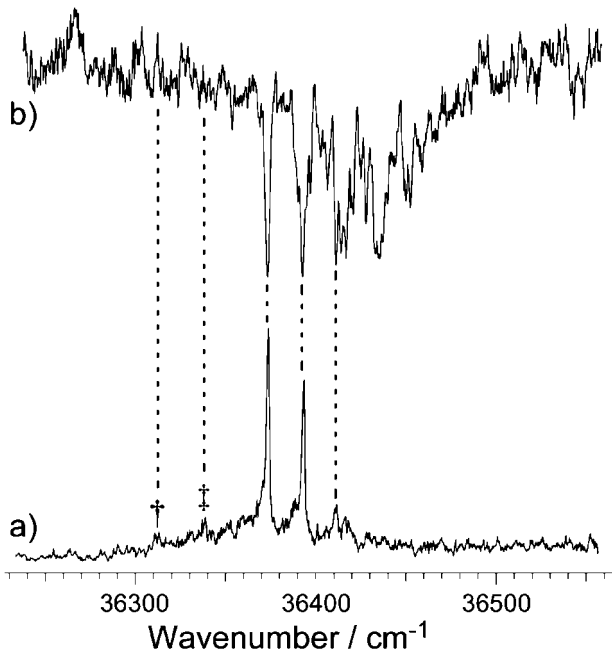

Figure 8. Comparison of a) REMPI and b) HB spectra of PhOH–Ar_3. Two bands indicated by † and ‡ in the REMPI spectrum a) are not observed in the HB spectrum b).

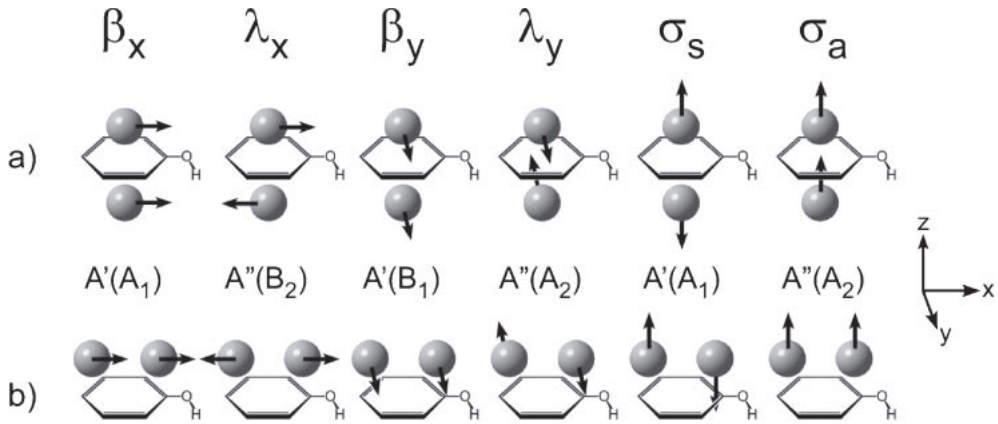

Figure 9. Intermolecular modes of a) (1|1) and b) (2|0) structures of PhOH–Ar_2. A′(A_1), etc. indicate the symmetries of each mode in the C_s (C_{2v}) point group.

Table 1. Frequencies (cm^{-1}) of Intermolecular Vibrations Observed in the HB Spectrum of PhOH–Ar_2 and Calculated for the (1|1) and (2|0) Structures

Mode	Obsd	Calcd (1|1)	Calcd (2|0)
β_x	14	17	9.9
λ_x	—	37	33
β_y	20	19	30
λ_y	—	61	6.1
σ_s	36	45	60
σ_a	—	67	54

combination with a progression in β_x. Based on σ_s, β_x, and β_y, we can assign all of the low-frequency bands in the HB spectrum of PhOH–Ar_2.

To support the assignments, the vibrational frequencies of the intermolecular modes in S_0 of PhOH–Ar_2 were also determined by ab initio MO calculations at the MP2/6-311++G(d,p) level using the Gaussian03 program.[25] The calculated frequencies for the (1|1) and (2|0) isomers are listed in Table 1 together with the frequencies observed in S_1. The order of the vibrational frequencies is well reproduced by both the (1|1) and the (2|0) isomers. The good reproduction of the experimental frequencies measured in S_1 by the calculated frequencies in S_0 suggests that the geometry and interaction energy of the cluster are not so changed along with the S_1–S_0 excitation. This conclusion is consistent with the observation that the S_1 origin is the strongest band in the REMPI spectrum and that the observed intermolecular progressions are short.

3.3 Additive Rules of S_1–S_0 Transition Energies. As mentioned in Section **3.1**, the S_1 origins of the predominant isomers at 36316, 36281, 36373, and 36338 cm^{-1} imply absolute shifts from $n = 0$ at 36350 cm^{-1} by −34, −69, +23, and −12 cm^{-1} for $n = 1$–4, respectively. The nearly additive red shifts for $n \leq 2$ are indicative of the (1|0) and (1|1) structures of PhOH–Ar and PhOH–Ar_2, whereas the absolute blue shift of the intense origin for $n = 3$ is indicative of the (3|0) isomer of PhOH–Ar_3.[22a,23] The weak origin at 36313 cm^{-1} indicated by † in Figure 8, corresponding to a total red shift of −37 cm^{-1}, is tentatively assigned in the present work to the hitherto unidentified (2|1) isomer of PhOH–Ar_3, by analogy with the isoelectronic aniline–Ar_n cluster series.[23] The HB spectrum of PhOH–Ar_3 is consistent with this view. Following the assignment given above, the addition of the first, second, and third Ar atom on a single side of PhOH induces incremental shifts of −34, +32, and +25 cm^{-1}, respectively. Figure 10 shows a schematic diagram of the additive rules, and Table 2 summarizes the observed S_1 origin energies and compares the experimental origin shifts from the phenol monomer with those extracted from the additive model. This simple scheme predicts the S_1 origin of the hitherto unidentified (2|0) isomer at ≈36348 cm^{-1} with essentially no total shift (−2 cm^{-1}), and indeed there is a relatively intense band in the corresponding REMPI spectrum of PhOH–Ar_2, which presumably corresponds to a different isomer from the predominant one as mentioned in the previous section.

The application of the above-mentioned additive rules to the $n = 4$ cluster predicts absolute shifts of −11 and −4 cm^{-1} for the (3|1) and (2|2) isomers, leading to expected S_1 origin bands at 36339 and 36346 cm^{-1}. Accordingly, the intense S_1 origin observed for PhOH–Ar_4 at 36338 cm^{-1} is attributed to the (3|1) isomer. As additional Ar atoms attached on the same side of PhOH induce incremental blue shifts for $n > 1$, the S_1 origin of the (4|0) isomer is expected to occur at frequencies larger than 36375 cm^{-1}.[22c] The broad background observed in the PhOH–Ar_4 spectrum is currently attributed to fragmentation of larger clusters after ionization.[5c] As can be seen in Table 2, the three input parameters, −34, +32, and +25 cm^{-1}, of the model can reproduce all six observed transition energies to within 1 cm^{-1}, strongly supporting the isomer assignments. Interestingly, the S_1 transition frequency of PhOH isolated in a cryogenic Ar matrix (36365 ± 15 cm^{-1})[26] is close to the gas phase value (36350 cm^{-1}), implying only a small shift of 15 ± 15 cm^{-1} induced by complete solvation of PhOH in an Ar environment.

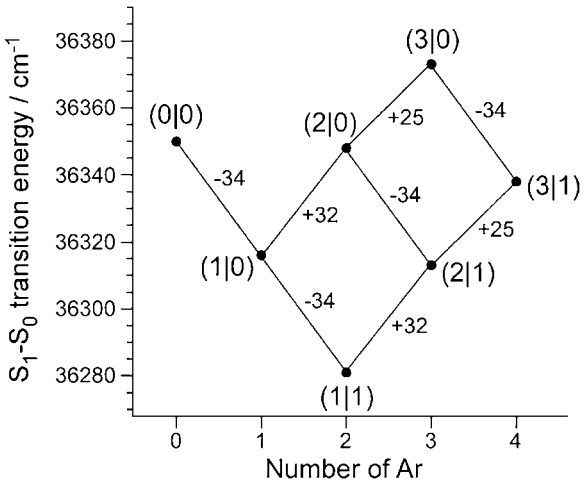

Figure 10. Additive rules of S_1–S_0 transition energies of π-bound PhOH–Ar_n with respect to the number of Ar and structures.

Table 2. Frequencies (cm^{-1}) of 0–0 Transitions of PhOH–Ar_n Observed in the REMPI Spectra, Differences from That of Phenol Monomer, Predicted by Additive Rules and Their Structural Assignments

n	0–0 transitions	Differences from monomer		Structural assignments
		Obsd	Model	
0	36350	0	0	—
1	36316	−34	−34	(1|0)
2	36281	−69	−68	(1|1)
	36348	−2	−2	(2|0)
3	36313	−37	−36	(2|1)
	36373	+23	+23	(3|0)
4	36338	−12	−11	(3|1)
	—	—	−4	(2|2)

3.4 Nanosecond IR Dip Spectra of Neutral Ground State. Based on the shifts of S_1–S_0 transition energy, we can discuss the structures of π-bound PhOH–Ar_n clusters, which however, is circumstantial evidence. It is not clear experimentally whether PhOH–Ar_n clusters really adopt π-bound structure. If PhOH–Ar_n clusters adopt H-bound structures, the vibrational frequency of OH stretching will be red-shifted. Thus, the OH

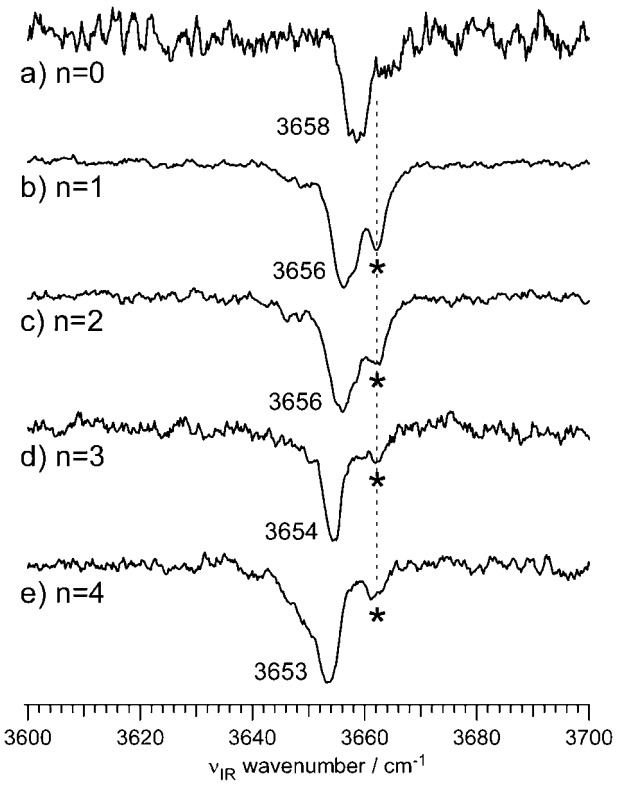

Figure 11. IR dip spectra of PhOH–Ar_n ($n = 0$–4) in the neutral ground state (S_0). Bands marked by * are assigned to combination bands anharmonic-coupling with OH stretching vibrations (refer to the manuscript).

stretching frequency is an indicator to discriminate π-bound or H-bound structures.

Figure 11 shows IR dip spectra of the OH stretching vibration (ν_{OH}) region of predominant isomers of PhOH–Ar_n ($n = 0$–4) in the neutral ground state with that of phenol monomer for comparison. To ionize each size of cluster, ν_{UV1} was fixed to the 0–0 band of the predominant isomer of each size, and ν_{UV2} was the same as that to measure the REMPI spectra.

The wavenumbers of the peaks, given in the figure, gradually shift to lower frequency with increase of Ar atoms. The small but noticeable shifts are consistent with the weak interaction of π-bound Ar with the OH bond. The significant total red shift of $-4\,cm^{-1}$ from ν_{OH} of phenol monomer for $n = 3$ may be taken as evidence for the close proximity of one of the Ar atoms and the OH group, which is expected for the (3|0) structure, that is an open sandwich structure of the Ar_3 triangle and phenol. Comparison with the corresponding shift of the H-bound PhOH–N_2 cluster, $-5\,cm^{-1}$,[6b] might also lead to the conclusion that one of the Ar atoms is H-bound, which is represented by PhOH–Ar_3(H/2π) hereafter. However, as mentioned in the previous section, the shift of S_1–S_0 transition energy points out the (3|0) structure. In addition, the recent photoionization and photofragmentation studies of PhOH–Ar_3 cluster clearly demonstrates that all Ar ligands are π-bound, i.e., PhOH–Ar_3(3π).[22a] Therefore, red shift of a few wavenumbers is comparative to the red shift of the H-bound PhOH–N_2 cluster, but it is premature to conclude H-bound structure only from such red shift.

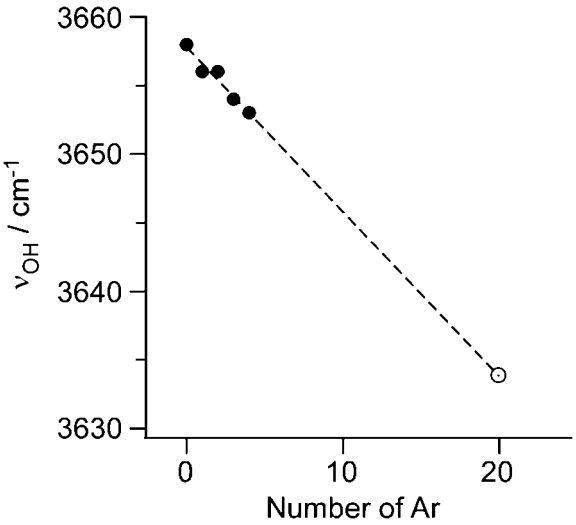

Figure 12. Size-dependency of the frequencies of ν_{OH} of PhOH–Ar_n in the neutral ground state (S_0). The open circle indicates the frequency of ν_{OH} of PhOH observed in an Ar matrix.[27] By extrapolating the observed red shifts, it is found that the red shift in the Ar matrix corresponds to $n \approx 20$ Ar atoms.

The monotonic red shift of OH stretching frequency with increase of Ar is shown in Figure 11. The frequency of ν_{OH} of PhOH observed in an Ar matrix at $3635\,cm^{-1}$ displays a red shift of $-23\,cm^{-1}$ from bare phenol, which is a significantly large shift.[27] Therefore, the interaction of PhOH with mainly the first Ar solvation shell is significantly enhanced upon the ν_{OH} vibration.[27] By extrapolating the observed red shifts, it is found that the red shift of $-23\,cm^{-1}$ corresponds to $n \approx 20$ Ar atoms (Figure 12). Thus, under the very crude assumption that each Ar atom in the first solvation shell generates roughly the same ν_{OH} shift and that only the first solvation shell contributes to the matrix shift, $n \approx 20$ Ar atoms can be accommodated around PhOH in this first shell. This size of the first solvation shell in PhOH–Ar_n is in good agreement with that derived previously for the aniline–Ar_n ($n = 22$) from mass spectrometry and electronic spectroscopy.[28]

There are further bands at the blue side of the main peaks, $3662\,cm^{-1}$, marked by an asterisk, which are independent of the number of Ar atoms, while the relative intensities with respect to each main peak go down with increase of the cluster size. These bands are assigned to a combination band, which is in anharmonic resonance with the fundamental of ν_{OH}. The decrease of the relative intensity can be explained by reducing the anharmonic interaction between the fundamental of ν_{OH} and the combination band, which is attributed to the red shift of the ν_{OH} with increase of Ar.

3.5 Nanosecond IR Dip Spectra of Cationic Ground State. Nanosecond IR dip spectra of the ν_{OH} region of $PhOH^+$–Ar_n ($n = 1$–4) are shown in Figure 13. Wavelengths of ν_{UV1} and ν_{UV2} were the same as those for the neutral ground state mentioned above. Wavenumbers of the observed peaks are given in the spectra. Two bands are observed at 3473 and $3537\,cm^{-1}$ for $n = 1$ cluster, while only one band in the vicinity of $3473\,cm^{-1}$ for $n = 2$–4 clusters. The frequency of ν_{OH} of phenol monomer cation is reported to be $3534\,cm^{-1}$,[11b]

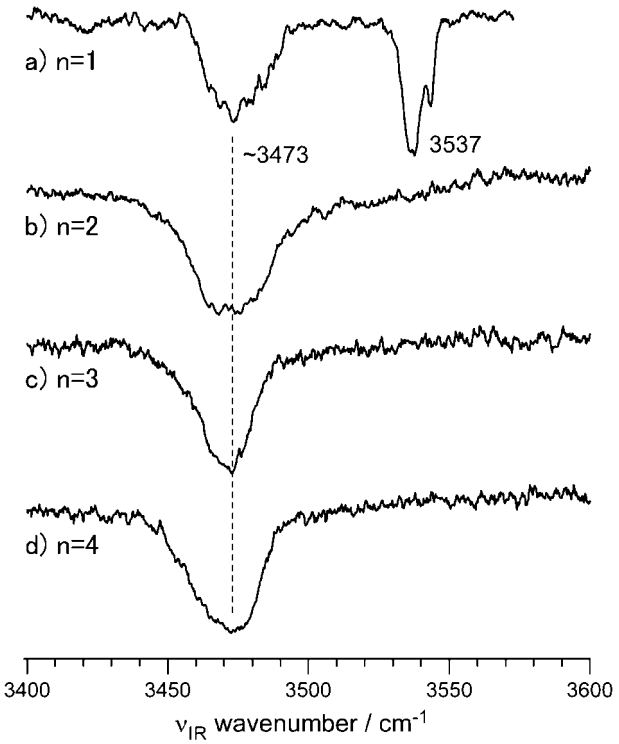

Figure 13. IR dip spectra of PhOH–Ar_n ($n = 1$–4) in the cationic ground state (D_0). A band observed at 3537 cm^{-1} is assigned to free ν_{OH} of π-bound structure, while bands around 3473 cm^{-1} is assigned to H-bonded ν_{OH} of H-bound structures.

thus the band observed at 3537 cm^{-1} for $n = 1$ is assigned to free ν_{OH} vibration of π-bound structure. On the other hand, the bands at $\approx$3473 cm^{-1} observed in all sizes are assigned to H-bonded ν_{OH} of H-bound structure, because the frequency of ν_{OH} of H-bound phenol–Ar_1 cluster cation, $PhOH^+$–Ar_1(H), which is the most stable structure in cationic state, is reported to be 3464 cm^{-1}.[12d] For comparison, the OH stretch of $PhOH^+$–N_2 cluster is observed at 3375 cm^{-1}, which is red-shifted 159 cm^{-1} from monomer cation, while 5 cm^{-1} in neutral ground state.[6b] Not as large as in H-bound $PhOH^+$–N_2, but also in $PhOH^+$–Ar_1(H), a large red shift of 61 cm^{-1} is observed, which means that the interaction between OH group and Ar atom is enhanced in the cationic state. This enhancement of the interaction can be explained by induced dipole of the Ar atom due to positive charge of phenol cation. The large red shift observed in H-bound $PhOH^+$–N_2 is explained by larger polarizability of N_2 than Ar.[12d] Therefore, the frequency of OH stretch is useful as a signature to determine whether $PhOH^+$–Ar_n cluster adopts π-bound or H-bound.

Here, we must pay notice that the H-bound structures are observed in all sizes despite π-bound structure in the neutral ground state, which clearly shows that $\pi \rightarrow$ H isomerization takes place through the ionization process. Because we excite PhOH–Ar_n clusters to S_1 state before ionization, the $\pi \rightarrow$ H isomerization should occur in the S_1 state or the cationic state. In fact, as mentioned in the introduction, we found that the $\pi \rightarrow$ H isomerization takes place in the cationic state by picosecond time-resolved IR spectroscopy, the details of which will be described in the next section.

Another curious point is that for all PhOH–Ar_n($n\pi$) clusters with $n \geq 2$, the $\pi \rightarrow$ H isomerization reaction leading to the formation of $PhOH^+$–Ar_n(H/[$n-1$]π) occurs with 100% efficiency, while the $n = 1$ cluster partially reacts. This phenomenon is deeply involved in the intramolecular vibrational redistribution (IVR) process after the $\pi \rightarrow$ H isomerization, which will be discussed later in account with the results of the time-resolved experiments.

3.6 Picosecond Time-Resolved IR Spectroscopy of $PhOH^+$–Ar_2. In order to clarify the state in which $\pi \rightarrow$ H isomerization takes place, time-resolved IR spectroscopy will provide a direct answer. By nanosecond IR spectroscopy, we can obtain geometric information of only the final reaction product of the $\pi \rightarrow$ H isomerization. Thus a shorter pulse laser system than nanosecond should be employed. To balance time resolution and energy resolution, a picosecond laser system is suitable for such experiment.

As mentioned in the previous section, it is expected that the $\pi \rightarrow$ H isomerization occurs in S_1 or cationic state. The experimental scheme to observe the dynamics is different for each state. We then considered that the $\pi \rightarrow$ H isomerization should take place in the cationic state because the electrostatic interaction would be drastically changed by generation of a charge due to the ionization. Based on this prediction, we tried to observe the dynamics in the cationic state of PhOH–Ar_2. The reason we chose $n = 2$ cluster at first is that 1) in $n = 1$ cluster, the reaction yield is not 100%, which will make the analysis complicated, 2) the distribution of populations of each size of clusters decreases with the cluster size, i.e., larger clusters have lower population, which makes the experiment difficult. Time-resolved experiments of other sizes are also investigated,[19a,29] however, they are now in progress, so in this review, only $n = 2$ cluster will be focused.

The experimental scheme for measuring the dynamics of $PhOH^+$–Ar_2 has already been described in Section **2**. To measure picosecond time-resolved IR dip spectra, the picosecond ν_{UV1} and ν_{UV2} lasers were fixed resonant to the S_1 origin transition of PhOH–Ar_2 (36282 cm^{-1}) and 32258 cm^{-1}, respectively, which corresponds to a total energy of IP + 550 cm^{-1}.

Figure 14 shows the resulting time-resolved IR spectra. The delay time between ν_{IR} and ν_{UV2} is indicated beside each spectrum. At 56 ps after the ionization, the IR spectrum is quite similar to the one measured by the nanosecond laser (Figure 13b), and only the H-bound ν_{OH} band was observed at $\approx$3467 cm^{-1}. When the delay time is shortened toward just after the ionization, the π-bound ν_{OH} band at 3537 cm^{-1} starts to appear at the delay time of $\approx$9 ps, and only the π-bound ν_{OH} transition is observed at 0 ps. These IR spectra demonstrate that the $PhOH^+$–Ar_2 is the π-bound structure just after the ionization, and one Ar atom migrates from the top of a benzene ring to the end of an OH group within the picosecond time scale. The spectra in Figure 14 thus provide direct evidence that the $\pi \rightarrow$ H isomerization occurs in the cationic ground state within a few ps after the ionization. In addition, this result also gives complete proof for PhOH–Ar_2 adopting π-bound structure in the neutral ground state. As mentioned in Section **3.4**, from the measurement of the frequency of ν_{OH} almost coinciding to free ν_{OH}, more precisely slightly red-

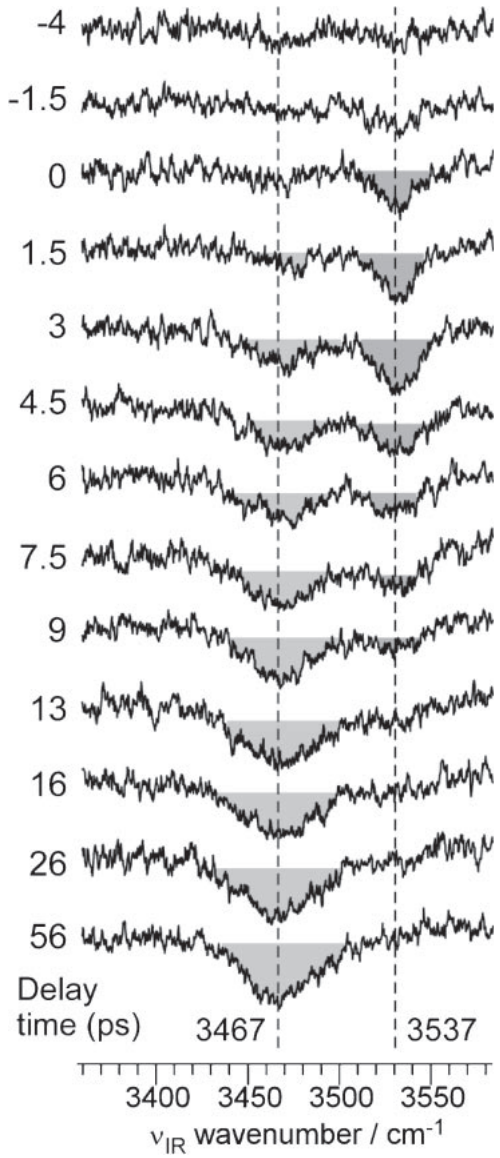

Figure 14. Picosecond time-resolved IR dip spectra of $PhOH^+$–Ar_2. Just after the ionization (0 ps), only free ν_{OH} (3537 cm^{-1}) is observed. With increasing the delay time, intensity of the free ν_{OH} decreases and red-shifted band appear at 3467 cm^{-1}, which is assigned to H-bonded ν_{OH}. This spectral change clearly demonstrates the $\pi \rightarrow$ H isomerization in $PhOH^+$–Ar_2.

shifted, it is difficult to determine whether PhOH–Ar_n clusters adopt π-bound or H-bound in the neutral ground state, because quite small red shift is expected even in the H-bound structure. The result of the picosecond experiment clearly shows that the structure just after the ionization, which should correspond to S_0 structure due to Franck–Condon principle, is π-bound.

To measure the time-evolution of the population of both the π-bound and the H-bound clusters of $PhOH^+$–Ar_2, ν_{IR} was fixed to the π-bound or H-bound ν_{OH} resonances (3537 or 3473 cm^{-1}, respectively), and the delay time between ν_{UV2} and ν_{IR} was scanned. Figure 15 shows the time-evolutions of the resulting ion dip signals for the π-bound and the H-bound structures. Here, the population of each structure was identified

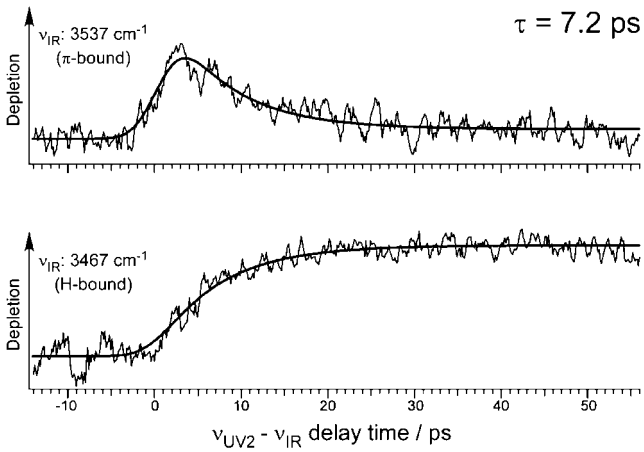

Figure 15. Time-evolution of the band intensities of π-bound and H-bound ν_{OH}s of $PhOH^+$–Ar_2. Both time-evolution can be fixed by single exponential functions with the same time constant of 7.2 ps which corresponds to that of the $\pi \rightarrow$ H isomerization in $PhOH^+$–Ar_2.

by the depletion of the ion signal at the corresponding ν_{OH} frequency. The vertical axis corresponds to the magnitude of the depletion. As can be seen in the figure, the π-bound structure is generated just after the ionization, and the population decays with increasing delay time. The population of the H-bound structure shows the opposite time-evolution. It increases gradually from zero directly after the ionization to a level that becomes almost constant after $\approx$50 ps.

To analyze the dynamics quantitatively, we considered a simple model, $\pi \xrightarrow{k}$ H, because the final reaction product is only H-bound structure in $n \geq 2$ clusters. Populations of each species are given by $[\pi] = [\pi]_0 \exp(-t/\tau)$, $[\mathrm{H}] = [\pi]_0\{1 - \exp(-t/\tau)\}$, where $\tau = 1/k$ and $[\pi]_0$ is an initial population of π-bound cluster cation. To fit the experimental time evolution, response function of our picosecond system should be considered. By nonresonant ionization detected (NID) IR spectroscopy,[15c,30] in which vibrationally excited phenol molecule by IR laser is ionized by nonresonant 2-photon absorption of UV laser, cross correlation of ν_{IR} and ν_{UV2} was measured and the full-width-of-half-maximum (FWHM) of the observed Gaussian cross correlation function was 5.4 ps. The observed time evolution of each structure is given by a convolution of the single exponential population and a Gaussian cross correlation function, $\exp[(-t/a)^2]$, where $2(\ln 2)^{1/2}a = 5.4$. The fitting functions are as following,

$$P_\pi(t) = A_\pi \exp\left(-\frac{t}{\tau} + \left(\frac{a}{2\tau}\right)^2\right) \cdot \mathrm{Erfc}\left(-\frac{t}{a} + \frac{a}{2\tau}\right) \quad (1)$$

$$P_\mathrm{H}(t) = A_\mathrm{H}\left[\mathrm{Erfc}\left(-\frac{t}{a}\right) - \exp\left(-\frac{t}{\tau} + \left(\frac{a}{2\tau}\right)^2\right) \cdot \mathrm{Erfc}\left(-\frac{t}{a} + \frac{a}{2\tau}\right)\right] \quad (2)$$

where Erfc is Gauss' error function, A_π and A_H are scaling factors. As a result of a least-squares analysis, we obtained the best fit at $\tau = 7.2$ ps for the time-evolution of both the π-bound and the H-bound structure. The calculated time-evolutions for both populations using $\tau = 7.2$ ps are also included in Figure 15 as solid lines. As can be seen, both experimental

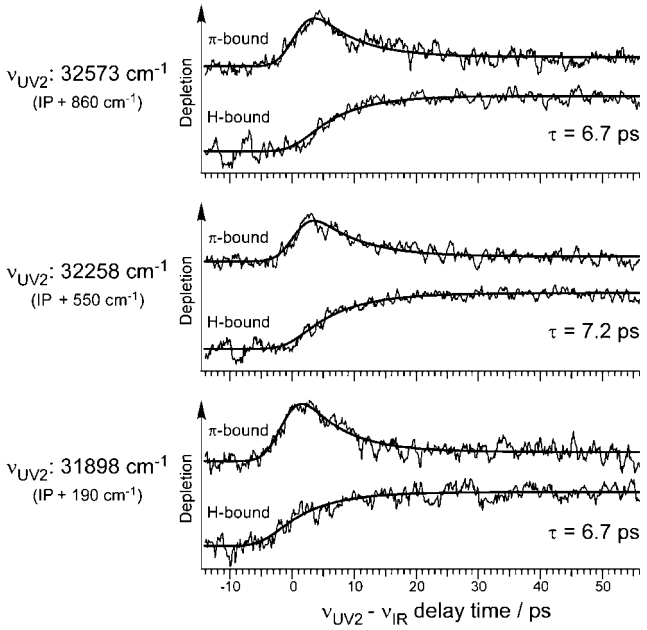

Figure 16. Excess energy dependence on the $\pi \rightarrow$ H isomerization of PhOH$^+$–Ar$_2$. In each excess energy, both decay and rise are fitted by the same time constant indicated in the figure.

time-evolutions are well reproduced by the same time constant. This means that the $\pi \rightarrow$ H isomerization is an elementary (i.e., single-step) reaction on the picosecond timescale.

Next, we investigated the excess energy dependence on the $\pi \rightarrow$ H isomerization by the picosecond real-time measurements. Figure 16 shows the time-evolutions of the π- and H-bound structures obtained when ν_{UV2} is fixed to 32573, 32258, and 31898 cm^{-1}, which gives excess energies of $E_{exc} = 860$, 550, and 190 cm^{-1} relative to the IP, respectively. Each time-evolution was fitted by the functions in eqs 1 and 2. The resulting time constants for the isomerization are 6.70 ± 0.60, 7.23 ± 0.70, and 6.67 ± 0.66 ps, respectively. These values are the same within the error bars, which suggests that the dynamics of the isomerization is relatively insensitive to the available excess energy (within the investigated range of $E_{exc} = 190$–860 cm^{-1}).

At this stage, it should be noted that E_{exc} involved in the ionization process is partitioned into vibrational energy of the cation and the kinetic energy of the ejected photoelectron, that is, not all E_{exc} is available for the isomerization process. The vibrational population distribution of the generated cations upon photoionization is given by the Franck–Condon factors and could be measured, for example, by high-resolution photoelectron spectroscopy (ZEKE and MATI). The MATI spectrum of PhOH$^+$–Ar$_2$ has been recently reported.[31] They measured only the intermolecular vibrational region 0–100 cm^{-1} above IP. In their spectrum obtained via zero vibrational level of S_1 state, harmonic progressions of β_x mode, which is in-phase sliding motion along C1–C4 axis of phenol, are observed with spacing of $\approx$10 cm^{-1}. The most intense level is β_x^3, and the levels from β_x^0 to β_x^7 are observed. For the intramolecular modes, some qualitative information can be derived from the corresponding spectra of bare PhOH$^+$,[32] because weakly π-bound Ar ligands have little influence on the intramolecular modes. Major vibrational peaks in the ZEKE spectrum of PhOH$^+$ within 850 cm^{-1} above the IP include the very intense absorptions at 0 (IP), 514 (ν_{6a}), and 808 cm^{-1} (ν_{12}), followed by somewhat weaker transitions at 348 (ν_{16a}), 411 (ν_{18b}), 557 (ν_{16b}), 608 (τ_{OH}), and 697 cm^{-1} ($2\nu_{16a}$).[32] Thus, at $E_{exc} = 190$ cm^{-1} no skeletal ring vibrations can be excited in PhOH$^+$–Ar$_2$, and the cluster cation is mainly populated in the vibrational ground state or some quanta of intermolecular mode (mainly β_x mode) up to about 100 cm^{-1}. At $E_{exc} = 550$ cm^{-1}, additional population can occur in the intramolecular states ν_{16a}, ν_{18b}, and ν_{6a}. At $E_{exc} = 860$ cm^{-1}, excitations of ν_{16b}, τ_{OH}, $2\nu_{16a}$, and ν_{12} are also feasible upon photoionization. In all cases, a certain degree of intermolecular excitation may accompany the intramolecular excitation.

The fact that isomerization is observed at $E_{exc} = 190$ cm^{-1} (Figure 16) implies that the ionization-induced isomerization occurs either from the ground vibrational state of π-bound PhOH$^+$–Ar$_2$ or from one of the low-frequency intermolecular modes ($<$100 cm^{-1}). As a consequence, the isomerization barrier is concluded to be quite low ($<$100 cm^{-1}). The nanosecond experiments suggest an even lower barrier ($<$46 cm^{-1}).[14] As the isomerization rate is almost unchanged when E_{exc} is raised up to 860 cm^{-1} (Figure 16), excitation of skeletal intramolecular ring modes are concluded to have no effect on the isomerization dynamics. In other words, the skeletal intramolecular ring modes do not couple with the isomerization coordinate. As a consequence, IVR from the intra molecular into the intermolecular degrees of freedom (in this paper, "IVR" includes vibrational redistribution within a whole cluster) must be slower than the isomerization dynamics. This scenario appears realistic, as the IVR lifetime of π-bound PhOH–Ar is still as long as 15 ps, even when the molecule is excited to the high-frequency ν_{OH} mode (3658 cm^{-1}).[33]

The characteristic features in the time-resolved IR dip spectra of PhOH$^+$–Ar$_2$ in Figure 14 is as follows. The first aspect is that the $\pi \rightarrow$ H isomerization does not have any back reaction, which might be expected for an isolated system because the reaction excess energy remains in the cluster. The lack of any back reaction can be explained by fast IVR after the isomerization. Namely, the internal excess energy generated by the isomerization to H-bound structure rapidly dissipates from the reaction coordinate to other vibrational modes. This energy loss process from the reaction coordinate will efficiently prevent any back reaction.

The second aspect is that the width of the H-bound ν_{OH} band is broader than that of π-bound one. In addition, closer inspection of the IR spectra in Figure 14 reveals that the width and position of the H-bound ν_{OH} band vary with the delay time. The broadening of the H-bound ν_{OH} transition is also observed in the nanosecond IR dip spectrum (Figure 13b). It is known that the ν_{OH} transition is broadened when the OH group acts as proton donor in an H-bond.[12b] However, it is not straightforward to explain why the width and the position of the band change dynamically. Another possibility for the broadening is the IVR process after the isomerization. After the IVR, the H-bound cluster cations populate various intermolecular vibrational states, which give rise to sequence hot band transitions superimposing the ν_{OH} fundamental transition.

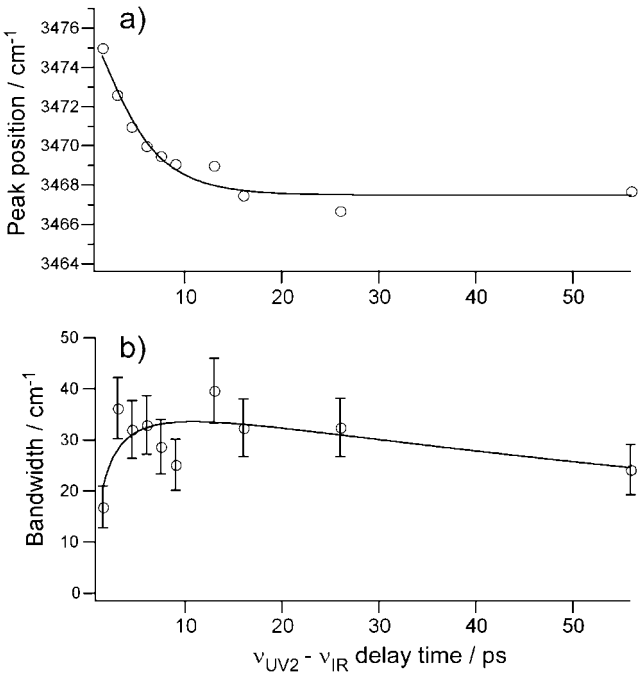

Figure 17. Time evolution of a) the peak position and b) the full width of half maximum of the H-bound ν_{OH} band observed in the picosecond time-resolved IR dip spectra of $PhOH^+$–Ar_2 shown in Figure 14.

In an effort to further elucidate the mechanism of the dynamic change of the band shape, we analyzed the contour of the H-bound ν_{OH} band in more detail. The band shape observed in the nanosecond IR dip spectrum (Figure 13b) can be fitted by a Lorentz function with a width of 24.6 cm^{-1}. The Lorentzian line shape is consistent with the existence of a rapid IVR process. On the other hand, the band contour in the picosecond IR dip spectra must be fitted by a Voigt function, which is a convolution of a Lorentzian (IVR lifetime) and a Gaussian, which accounts for the reduced spectral resolution. The picosecond IR dip spectrum obtained at 56 ps was fitted by the Voigt function in which the bandwidth of the Lorentzian is fixed to the value obtained from the nanosecond IR dip spectrum (24.6 cm^{-1}), and as a result the bandwidth (FWHM) of the Gaussian was obtained as 29.1 cm^{-1}. Finally, we fitted all other H-bound ν_{OH} bands to the Voigt function by keeping the bandwidth of the Gaussian fixed to 29.1 cm^{-1} and obtained the peak position and the bandwidth of the Lorentzian for each of the bands. Figure 17a shows the time-evolution of the peak position. It was found that the peak position shows a single-exponential convergence from 3475 to 3467 cm^{-1}. By fitting the time-evolution of the peak position to the convolution of a single exponential and the Gaussian cross correlation function (FWHM = 5.4 ps), a time constant of 4.1 ps was obtained. The time-evolution of the bandwidth is shown in Figure 17b with error bars. There is a certain amount of fluctuation, however, it seems that the bandwidth slightly decreases following the initial broadening.

To explain the dynamic change of the band shape, we develop a simple model to rationalize the origin of the peak shift and the variation of the bandwidth. The H-bound $PhOH^+$–Ar_2 cluster cation produced by the isomerization of the π-bound structure is internally "hot," i.e., it remains at vibrationally excited states, denoted ν_x. Therefore, the observed ν_{OH} band of the H-bound structure is a superposition of a sequence hot bands of the type $\nu_{OH} + \nu_x \leftarrow \nu_x$. Their transition frequencies are almost equal to the frequency of pure ν_{OH}, but, due to variations in anharmonicity, slightly different by ν_x. Thus, the observed ν_{OH} band contour reflects a distribution of the vibrationally excited states ν_x produced by the $\pi \rightarrow H$ isomerization, and the peak shift exhibits a change of this distribution. Figure 18a shows a schematic diagram of the implications of this sequential IVR model on the peak shift. In this scheme, to distinguish the various vibrationally excited H-bound structures, they are represented by H_n ($n = 0, 1, \ldots$). If the vibrational ν_{OH} frequencies of H_n are gradually shifting to the red and the red shift converges to a certain frequency, the peak shift can be explained by the sequential transition (or IVR), such as $\pi \rightarrow H_0 \rightarrow H_1 \rightarrow H_2 \rightarrow \ldots$ and so on. As shown in the figure, this simple model can also qualitatively account for the time-evolution of the bandwidth (Figure 18b). Within this model, the band broadening at early stage of the reaction is due to the monotonic red shift through the IVR process, and the decrease of the bandwidth derives from the convergence of the red shift.

As mentioned above, the time constant for this peak shift was obtained to be 4.1 ps, which, however, does not correspond to the time constant of the IVR process, because the convergence of the peak shift does not correlate with the termination of the IVR process. In addition, the convergence of the peak shift is faster than the $\pi \rightarrow H$ isomerization ($\approx$7 ps). This can be explained by the IVR process after the convergence of the peak shift, i.e., as shown in Figure 18, even if the peak shift converges, H_0–H_4 transfer to the terminal position by the IVR process and the peak height increases more than before. Thus, the IVR process occurs even after the convergence of the peak shift, and this is a reason that the time constant for the $\pi \rightarrow H$ isomerization is larger than that for the peak shift.

3.7 Isomerization Dynamics in $n = 1$ and 3 Clusters. For $n = 3$ cluster, we reported results of time-resolved experiments recently.[19a] Briefly, even just after the ionization, π-bound ν_{OH} cannot be observed, and therefore the $\pi \rightarrow H$ isomerization may be faster than the time-resolution of our picosecond setup. Such very fast isomerization may be explained by its structure. As mentioned in Section **3.3**, the predominant isomer of the $n = 3$ cluster in the neutral ground state presumably adopts (3|0) structure. In this structure, one Ar atom probably exists near the OH group because three Ar atoms are dished up on the one side of the benzene ring, thus it will easily isomerize to H-bound structure. In addition, the back-reaction is not observed, which is probably because of the IVR process similar to $n = 2$ cluster.

For $n = 1$ cluster, unfortunately, data for time-resolved IR spectra have not been established yet. As mentioned in Section **3.5**, because the yield of the $\pi \rightarrow H$ isomerization in $n = 1$ cluster is not 100%, both ν_{OH} of π-bound and H-bound structures are observed simultaneously in the time-resolved IR spectra, which are difficult to be completely separated in our spectral resolution ($\approx$30 cm^{-1}). The band separation between π-bound and H-bound ν_{OH} is larger in $PhOH^+$–Kr_1 than

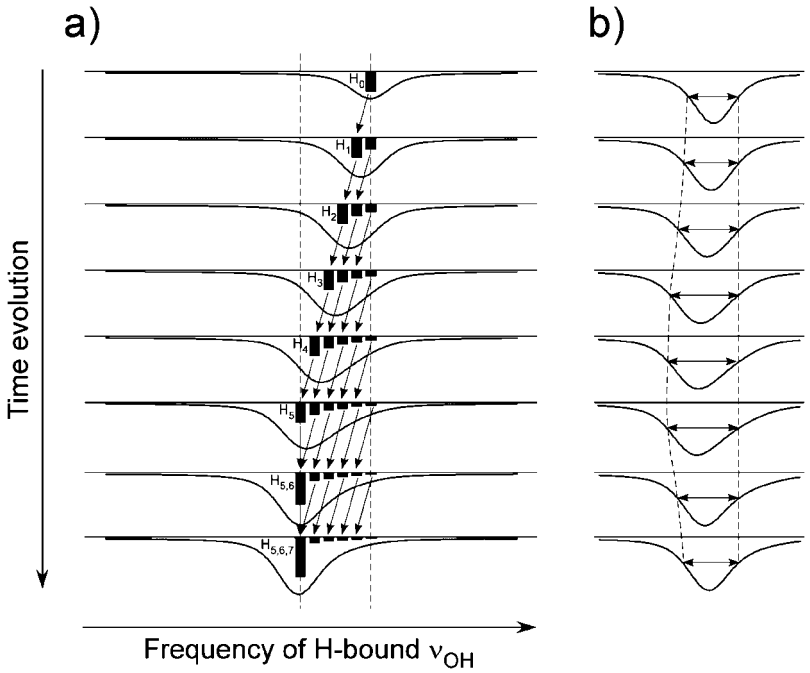

Figure 18. Schematic diagram of the mechanisms of a) the peak shift and b) the change of the bandwidth of the H-bound ν_{OH} band in $PhOH^+$–Ar_2 due to the $\pi \rightarrow$ H isomerization.

$PhOH^+$–Ar_1, thus we measured time-resolved IR spectra of $PhOH^+$–Kr_1 cluster, in which both ν_{OH} are observed in the final stage of the isomerization, and obtained the time constant of 20 ps for the $\pi \rightarrow$ H isomerization.[29] Also in $PhOH^+$–Kr_1 clusters, the ν_{OH} of the π-bound and H-bound structures are simultaneously observed in the nanosecond IR spectra. Because the initial state of the reaction is a single state, which means that we can experimentally prepare a single state for the reaction, it is impossible that a part of it causes the $\pi \rightarrow$ H isomerization. Instead, it is natural to consider the back reaction, i.e., an equilibrium between the π- and H-bound structures is achieved by H $\rightarrow \pi$ isomerization. Differently from the larger clusters, the $n = 1$ cluster has only 3 intermolecular modes, which leads to low density of state in the vibrationally excited H-bound structure. Thus it is expected that the efficient IVR process which deactivates the back reaction does not occur. If this interpretation is correct, it is expected that no back reaction should be observed in phenol/polyatomic molecule (1:1) cluster cation, because such a cluster has 6 intermolecular modes which cause high density of state. In fact, we measured phenol/methane (1:1) cluster cation, and observed only H-bound structure by nanosecond experiment.

In $PhOH^+$–Ar_1 and $PhOH^+$–Kr_1 clusters, the excess energy dependency of the $\pi \rightarrow$ H isomerization has been investigated precisely.[34] According to the results, even when the cations at zero vibrational level are generated by threshold ionization, ν_{OH} of H-bound structure is observed, which means that the $\pi \rightarrow$ H isomerization has a quite low barrier (a few wavenumbers). This result is bothering us, because it is completely conflicting with the aspects of the intermolecular potential obtained by ZEKE spectroscopy.[5c] We are cognizant that this is the most serious outstanding issue to be solved, which will be discussed in the final section.

4. Conclusion Remarks and Remaining Problems

In this paper, I reviewed structural and dynamic studies of phenol/Ar clusters and their cations in accord with recent results.

At first, static structures of phenol/Ar (1:1–4) clusters in the neutral ground state are described on the basis of electronic and vibrational spectra. To predict the geometries of π-bound structures, the additive rules of S_1–S_0 transition energies were introduced and the predominant isomers of each size are assigned to (1|0), (1|1), (3|0), and (3|1), respectively.

Also for the cationic ground state, we measured IR spectra of OH stretching, ν_{OH}, region and observed two bands at 3473 and 3537 cm^{-1} for $n = 1$ cluster, while only a red one was observed in larger clusters. The blue band coincides to the frequency of free ν_{OH} observed in phenol monomer cation.[11b] On the other hand, the red ones correspond to ν_{OH} of H-bound $PhOH^+$–Ar_1 which is the most stable structure in the cationic state.[12d] Therefore we concluded that both π-bound and H-bound structures are observed in the $n = 1$ cluster cation, while only H-bound structure in $n \geq 2$ cluster cations. This result is surprising for us, because PhOH–Ar_n ($n = 1$–4) in the neutral ground state adopt the π-bound structure and relatively sharp ionization threshold are observed in $n = 1$ and 2 clusters, which leads an expectation that the π-bound structure should be produced by laser ionization according to the Franck–Condon principle. We thought that such drastic structural change should occur in the cationic state because of charge generation on the benzene ring.

To confirm that the $\pi \rightarrow$ H isomerization occurs in in the cationic state, we applied picosecond time-resolved IR spectroscopy to $PhOH^+$–Ar_2 cluster. At about 50 ps after the laser ionization, only H-bound ν_{OH} is observed similarly to the nanosecond experiments, while only π-bound ν_{OH} is observed

just after the ionization. By changing the delay time between the laser ionization and IR measurement, we can observe that π-bound ν_{OH} changes to H-bound ν_{OH} gradually within about 10 ps. By analyzing the time evolution of IR band intensity of each structure, it was found that the time constant of the $\pi \rightarrow$ H isomerization is 7.2 ps and it is a single-step reaction within the picosecond time scale. In addition, we found a dynamic peak shift and changing of the bandwidth of H-bound ν_{OH}. To explain these spectral changes, we considered a simple sequential IVR model and interpreted that their aspects show the IVR process in vibrationally excited H-bound structure generated by the $\pi \rightarrow$ H isomerization.

In this paper, time-resolved IR spectra of only $PhOH^+$–Ar_2 cluster were reviewed, however, the results of other sizes, $n = 1$ and 3, are analyzed now (the result of $n = 3$ has been reported recently[19a]). Anyway, the time-resolved experiments will reveal the $\pi \rightarrow$ H isomerization in the cationic state also for other sizes. However we are confronting an awkward problem of how to interpret intermolecular vibrations in especially $n = 1$ and 2 cluster cations because they show clear transitions to some intermolecular modes despite the large amplitude dynamics of the $\pi \rightarrow$ H isomerization. Especially, the problem in the $n = 1$ cluster cation is serious. Müller-Dethlefs and co-workers reported ZEKE spectra of $PhOH^+$–Ar_1 clusters, in which they assigned 3 intermolecular modes based on the π-bound structure.[5c] The number of the intermolecular modes, 3, corresponds to the degree of freedom of Ar atom, thus the observation of the 3 intermolecular modes means that motion of Ar atom can be spectroscopically described completely. According to their assignment, Ar atom sits on the benzene ring, i.e., the $\pi \rightarrow$ H isomerization is impossible or has a very high barrier, both of which conflict with our results. Of course, when they published that paper, the $\pi \rightarrow$ H isomerization had not been found yet, and they achieved their best for the analysis at that time. In addition, even now, their assignments are not unnatural from the spectroscopic view except a conflict with the $\pi \rightarrow$ H isomerization dynamics. Because both experimental results, ZEKE spectra and our time-resolved spectra, are undoubted, and our interpretation for the time-resolved experiments is hardly demolished, therefore we should reconsider the assignments for the ZEKE spectra, i.e., intermolecular modes of $PhOH^+$–Ar_1, with taking account of the large amplitude motion of the $\pi \rightarrow$ H isomerization. If one considers the $\pi \rightarrow$ H isomerization as an anharmonic large amplitude vibrational mode, the normal mode view for the intermolecular vibration between Ar atom and phenol cation collapses, because the intermolecular potential cannot be described by the sum of three unary functions any more. For instance, because the binding energy of Ar atom is larger in the H-bound structure than the π-bound, the frequency of the intermolecular stretching mode largely depends on the position of Ar atom. It means that the intermolecular stretching mode strongly couples to the isomerization coordinate. The situation is the same between the intermolecular sliding mode and the isomerization coordinate. Therefore, three-dimensional Schrödinger equation should be directly solved without variable separation to obtain energy levels of intermolecular vibrations. For such an analysis, three-dimensional potential energy surface (PES) is necessary. However, interaction energy between Ar atom and phenol cation is very sensitive with respect to calculation levels, thus high level and expensive calculations should be necessary to obtain a quantitatively dependable PES. Such an effort is now in progress not only by us but also by other theoreticians.[8d,35]

If we reconsider the $\pi \rightarrow$ H isomerization from such a viewpoint, i.e., regarding the dynamics of the isomerization as intermolecular large amplitude vibrations, one question arises, "Can we interpret the two OH stretching bands as π-bound ν_{OH} and H-bound ν_{OH}, respectively?" Namely, if the $\pi \rightarrow$ H isomerization takes place, it means that $PhOH^+$–Ar_1 stays at a certain vibrational level whose wavefunction diffuses all around the $PhOH^+$ molecule, which suggests that the π-bound and H-bound structures cannot be discriminated with quantum mechanical sense. In other words, we cannot regard the two OH vibrational transitions as rising up within the static π-bound and H-bound structures, respectively. In such a situation, also a potential function of the OH stretching cannot be separated from the intermolecular potential function, any more. Therefore, more precisely, we must consider a potential function of 4 variables (3 variables of the coordinates of Ar atom and 1 variable of the OH stretching coordinate) to describe energy levels concerning the OH stretching motion.

At a glance, the phenol/Ar cluster seems a very simple system, however, it has quite curious dynamics and also still has several puzzles. To figure out the puzzles, precise quantum mechanical treatments should be applied, for which it is never a simple system. In that way, it is not an exaggeration to say that the phenol/Ar cluster system is a touchstone for fundamental physical chemistry, how to understand multidimensional atomic motions.

This study was supported in part by a Grant-in-Aid for Scientific Research KAKENHI in the priority area "Molecular Science for Supra Functional Systems" from the Ministry of Education, Culture, Sports, Science and Technology (MEXT) Japan, and the Core-to-Core Program of the Japan Society for Promotion of Science. Author thanks Prof. M. Fujii (Tokyo Tech), Prof. K. Müller-Dethlefs (Manchester Univ.), Prof. O. Dopfer (TU Berlin), Prof. M. Sakai (Tokyo Tech), and Dr. M. Miyazaki (Tokyo Tech) for stimulating discussion and helpful comments in this work.

References

1 R. Shimada, H. Hamaguchi, *J. Chem. Phys.* **2011**, *134*, 034516.

2 a) G. A. Jeffrey, W. Saenger, *Hydrogen Bonding in Biological Systems*, Springer, Heidelberg, **1991**. b) M. B. Smith, J. March, *Advanced Organic Chemistry: Reactions, Mechanisms, and Structure*, 5th ed., Wiley, New York, **2001**. c) L. Stryer, *Biochemistry*, 4th ed., Freeman, New York, **1996**. d) J. A. Subirana, M. Soler-López, *Annu. Rev. Biophys. Biomol. Struct.* **2003**, *32*, 27. e) M. M. Teeter, *Annu. Rev. Biophys. Biophys. Chem.* **1991**, *20*, 577. f) T. S. Zwier, *J. Phys. Chem. A* **2001**, *105*, 8827. g) B. Brutschy, *Chem. Rev.* **1992**, *92*, 1567. h) A. W. Castleman, Jr., S. Wei, *Annu. Rev. Phys. Chem.* **1994**, *45*, 685. i) E. A. Meyer, R. K. Castellano, F. Diederich, *Angew. Chem., Int. Ed.* **2003**, *42*, 1210.

3 a) E. J. Bieske, O. Dopfer, *Chem. Rev.* **2000**, *100*, 3963.

b) A. W. Castleman, in *Clusters of Atoms and Molecules II*, ed. by H. Haberland, Springer, Berlin, **1994**, Vol. 56, p. 77. c) M. A. Duncan, *Int. Rev. Phys. Chem.* **2003**, *22*, 407. d) K. Müller-Dethlefs, P. Hobza, *Chem. Rev.* **2000**, *100*, 143. e) W. H. Robertson, M. A. Johnson, *Annu. Rev. Phys. Chem.* **2003**, *54*, 173. f) K. Müller-Dethlefs, O. Dopfer, T. G. Wright, *Chem. Rev.* **1994**, *94*, 1845.

4 N. Gonohe, H. Abe, N. Mikami, M. Ito, *J. Phys. Chem.* **1985**, *89*, 3642.

5 a) E. J. Bieske, M. W. Rainbird, I. M. Atkinson, A. E. W. Knight, *J. Chem. Phys.* **1989**, *91*, 752. b) M. S. Ford, S. R. Haines, I. Pugliesi, C. E. H. Dessent, K. Müller-Dethlefs, *J. Electron Spectrosc. Relat. Phenom.* **2000**, *112*, 231. c) S. R. Haines, C. E. H. Dessent, K. Müller-Dethlefs, *J. Electron Spectrosc. Relat. Phenom.* **2000**, *108*, 1. d) M. Mons, J. Le Calvé, F. Piuzzi, I. Dimicoli, *J. Chem. Phys.* **1990**, *92*, 2155. e) M. Schmidt, M. Mons, J. Le Calvé, *Z. Phys. D: At., Mol. Clusters* **1990**, *17*, 153.

6 a) T. Ebata, A. Iwasaki, N. Mikami, *J. Phys. Chem. A* **2000**, *104*, 7974. b) A. Fujii, M. Miyazaki, T. Ebata, N. Mikami, *J. Chem. Phys.* **1999**, *110*, 11125.

7 G. V. Hartland, B. F. Henson, V. A. Venturo, P. M. Felker, *J. Phys. Chem.* **1992**, *96*, 1164.

8 a) C. E. H. Dessent, K. Müller-Dethlefs, *Chem. Rev.* **2000**, *100*, 3999. b) J. Makarewicz, *J. Chem. Phys.* **2006**, *124*, 08431. c) F. Tran, T. A. Wesołowski, *Int. J. Quantum Chem.* **2005**, *101*, 854. d) J. Černý, X. Tong, P. Hobza, K. Müller-Dethlefs, *J. Chem. Phys.* **2008**, *128*, 114319.

9 a) C. E. H. Dessent, S. R. Haines, K. Müller-Dethlefs, *Chem. Phys. Lett.* **1999**, *315*, 103. b) X. Zhang, J. L. Knee, *Faraday Discuss.* **1994**, *97*, 299.

10 A. Fujii, T. Sawamura, S. Tanabe, T. Ebata, N. Mikami, *Chem. Phys. Lett.* **1994**, *225*, 104.

11 a) T. Ebata, A. Fujii, N. Mikami, *Int. Rev. Phys. Chem.* **1998**, *17*, 331. b) A. Fujii, A. Iwasaki, T. Ebata, N. Mikami, *J. Phys. Chem. A* **1997**, *101*, 5963.

12 a) O. Dopfer, *Z. Phys. Chem.* **2005**, *219*, 125. b) N. Solcà, O. Dopfer, *Chem. Phys. Lett.* **2000**, *325*, 354. c) N. Solcà, O. Dopfer, *J. Mol. Struct.* **2001**, *563–564*, 241. d) N. Solcà, O. Dopfer, *J. Phys. Chem. A* **2001**, *105*, 5637. e) N. Solcà, O. Dopfer, *Chem. Phys. Lett.* **2003**, *369*, 68.

13 a) H. S. Andrei, N. Solcà, O. Dopfer, *Phys. Chem. Chem. Phys.* **2004**, *6*, 3801. b) H. S. Andrei, N. Solcà, O. Dopfer, *J. Phys. Chem. A* **2005**, *109*, 3598. c) N. Solcà, O. Dopfer, *Eur. Phys. J. D* **2002**, *20*, 469. d) N. Solcà, O. Dopfer, *Phys. Chem. Chem. Phys.* **2004**, *6*, 2732. e) F. M. Pasker, N. Solcà, O. Dopfer, *J. Phys. Chem. A* **2006**, *110*, 12793. f) N. Solcà, O. Dopfer, *Chem. Phys. Lett.* **2001**, *342*, 191. g) N. Solcà, O. Dopfer, *J. Am. Chem. Soc.* **2004**, *126*, 1716. h) N. Solcà, O. Dopfer, *J. Chem. Phys.* **2004**, *120*, 10470.

14 S. Ishiuchi, M. Sakai, Y. Tsuchida, A. Takeda, Y. Kawashima, O. Dopfer, K. Müller-Dethlefs, M. Fujii, *J. Chem. Phys.* **2007**, *127*, 114307.

15 a) S. Ishiuchi, M. Sakai, K. Daigoku, K. Hashimoto, M. Fujii, *J. Chem. Phys.* **2007**, *127*, 234304. b) S. Ishiuchi, K. Daigoku, K. Hashimoto, M. Fujii, *J. Chem. Phys.* **2004**, *120*, 3215. c) M. Sakai, S. Ishiuchi, M. Fujii, *Eur. Phys. J. D* **2002**, *20*, 399. d) S. Ishiuchi, K. Daigoku, M. Saeki, M. Sakai, K. Hashimoto, M. Fujii, *J. Chem. Phys.* **2002**, *117*, 7077. e) S. Ishiuchi, K. Daigoku, M. Saeki, M. Sakai, K. Hashimoto, M. Fujii, *J. Chem. Phys.* **2002**, *117*, 7083. f) S. Ishiuchi, M. Sakai, K. Daigoku, T. Ueda, T. Yamanaka, K. Hashimoto, M. Fujii, *Chem. Phys. Lett.* **2001**, *347*, 87.

16 S. Ishiuchi, M. Sakai, Y. Tsuchida, A. Takeda, Y. Kawashima, M. Fujii, O. Dopfer, K. Müller-Dethlefs, *Angew. Chem., Int. Ed.* **2005**, *44*, 6149.

17 U. Graf, H. Niikura, S. Hirayama, *Rev. Sci. Instrum.* **1996**, *67*, 406.

18 T. Ebata, in *Nonlinear Spectroscopy for Molecular Structure Determination*, ed. by R. W. Field, E. Hirota, J. P. Maier, S. Tsuchiya, Blackwell Science, **1998**.

19 a) S. Ishiuchi, M. Miyazaki, M. Sakai, M. Fujii, M. Schmies, O. Dopfer, *Phys. Chem. Chem. Phys.* **2011**, *13*, 2409. b) S. Ishiuchi, Y. Tsuchida, O. Dopfer, K. Müller-Dethlefs, M. Fujii, *J. Phys. Chem. A* **2007**, *111*, 7569.

20 a) M. Schmitt, C. Ratzer, W. L. Meerts, *J. Chem. Phys.* **2004**, *120*, 2752. b) A. Sur, P. M. Johnson, *J. Chem. Phys.* **1986**, *84*, 1206.

21 D. Bahat, O. Cheshnovsky, U. Even, N. Lavie, Y. Magen, *J. Phys. Chem.* **1987**, *91*, 2460.

22 a) A. Armentano, M. Riese, M. Taherkhani, M. Ben Yezzar, K. Müller-Dethlefs, M. Fujii, O. Dopfer, *J. Phys. Chem. A* **2010**, *114*, 11139. b) I. Kalkman, C. Brand, T.-B. C. Vu, W. L. Meerts, Y. N. Svartsov, O. Dopfer, X. Tong, K. Müller-Dethlefs, S. Grimme, M. Schmitt, *J. Chem. Phys.* **2009**, *130*, 224303. c) M. Schmidt, M. Mons, J. Le Calvé, *Chem. Phys. Lett.* **1991**, *177*, 371.

23 a) S. Douin, S. Piccirillo, P. Bréchignac, *Chem. Phys. Lett.* **1997**, *273*, 389. b) P. Hermine, P. Parneix, B. Coutant, F. G. Amar, Ph. Bréchignac, *Z. Phys. D: At., Mol. Clusters* **1992**, *22*, 529.

24 S. Douin, P. Hermine, P. Parneix, P. Brechignac, *J. Chem. Phys.* **1992**, *97*, 2160.

25 M. J. Frisch, G. W. Trucks, H. B. Schlegel, G. E. Scuseria, M. A. Robb, J. R. Cheeseman, J. A. Montgomery, Jr., T. Vreven, K. N. Kudin, J. C. Burant, J. M. Millam, S. S. Iyengar, J. Tomasi, V. Barone, B. Mennucci, M. Cossi, G. Scalmani, N. Rega, G. A. Petersson, H. Nakatsuji, M. Hada, M. Ehara, K. Toyota, R. Fukuda, J. Hasegawa, M. Ishida, T. Nakajima, Y. Honda, O. Kitao, H. Nakai, M. Klene, X. Li, J. E. Knox, H. P. Hratchian, J. B. Cross, V. Bakken, C. Adamo, J. Jaramillo, R. Gomperts, R. E. Stratmann, O. Yazyev, A. J. Austin, R. Cammi, C. Pomelli, J. W. Ochterski, P. Y. Ayala, K. Morokuma, G. A. Voth, P. Salvador, J. J. Dannenberg, V. G. Zakrzewski, S. Dapprich, A. D. Daniels, M. C. Strain, O. Farkas, D. K. Malick, A. D. Rabuck, K. Raghavachari, J. B. Foresman, J. V. Ortiz, Q. Cui, A. G. Baboul, S. Clifford, J. Cioslowski, B. B. Stefanov, G. Liu, A. Liashenko, P. Piskorz, I. Komaromi, R. L. Martin, D. J. Fox, T. Keith, M. A. Al-Laham, C. Y. Peng, A. Nanayakkara, M. Challacombe, P. M. W. Gill, B. Johnson, W. Chen, M. W. Wong, C. Gonzalez, J. A. Pople, *Gaussian 03 (Revision C.02)*, Gaussian, Inc., Wallingford CT, **2004**.

26 C. Crépin, A. Tramer, *Chem. Phys.* **1991**, *156*, 281.

27 A. M. Plokhotnichenko, E. D. Radchenko, Yu. P. Blagoĭ, V. A. Karachevtsev, *Low Temp. Phys.* **2001**, *27*, 666.

28 T. Pino, P. Parneix, S. Douin, Ph. Bréchignac, *J. Phys. Chem. A* **2004**, *108*, 7364.

29 M. Miyazaki, A. Takeda, S. Ishiuchi, M. Sakai, O. Dopfer, M. Fujii, *Phys. Chem. Chem. Phys.* **2011**, *13*, 2744.

30 a) S. Ishiuchi, H. Shitomi, K. Takazawa, M. Fujii, *Chem. Phys. Lett.* **1998**, *283*, 243. b) T. Omi, H. Shitomi, N. Sekiya, K. Takazawa, M. Fujii, *Chem. Phys. Lett.* **1996**, *252*, 287.

31 X. Tong, A. Armentano, M. Riese, M. BenYezzar, S. M. Pimblott, K. Müller-Dethlefs, S. Ishiuchi, M. Sakai, A. Takeda, M. Fujii, O. Dopfer, *J. Chem. Phys.* **2010**, *133*, 154308.

32 a) O. Dopfer, Ph.D. Thesis, Technische Universität München, **1994**. b) O. Dopfer, G. Reiser, K. Müller-Dethlefs,

E. W. Schlag, S. D. Colson, *J. Chem. Phys.* **1994**, *101*, 974.
33 Y. Yamada, Y. Katsumoto, T. Ebata, *Phys. Chem. Chem. Phys.* **2007**, *9*, 1170.
34 A. Takeda, H.-S. Andrei, M. Miyazaki, S. Ishiuchi, M. Sakai, M. Fujii, O. Dopfer, *Chem. Phys. Lett.* **2007**, *443*, 227.
35 a) J. Černý, X. Tong, P. Hobza, K. Müller-Dethlefs, *Phys. Chem. Chem. Phys.* **2008**, *10*, 2780. b) Ch. Walter, R. Kritzer, A. Schubert, C. Meier, O. Dopfer, V. Engel, *J. Phys. Chem. A* **2010**, *114*, 9743. c) K. Nakamura, K. Hoki, K. Sato, K. Tsuneda, H. Kono, Annual Meeting of Japan Society for Molecular Science, Osaka, **2010**, Abstr. No. 4P067.

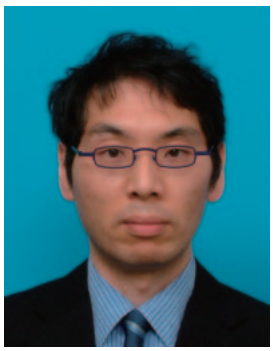

Shun-ichi Ishiuchi was born in 1973 in Shizuoka, Japan. He received a Ph.D. from Graduate University for Advanced Studies, Institute for Molecular Science in 2001. During the doctoral program, he was selected as a Research Fellow of the Japan Society for the Promotion of Science (1998–2001). After that, he built his academic carrier as a Research Associate of Faculty of Science and Technology, Keio University (2001–2003) and a Researcher of Precursory Research for Embryonic Science and Technology, Japan Science and Technology Agency (2002–2006), and is currently an Assistant Professor of Chemical Spectroscopy Division, Chemical Resources Laboratory, Tokyo Institute of Technology (2004–). He received Seiichi Tejima Research Award (2007) at "Real-time Observation of Ionization-Induced Hydrophobic to Hydrophilic Switching" and the Chemical Society of Japan Award for Young Chemists (2008) at "Development of Multiresonance Laser Spectroscopy for Tracing Reactions and Study of New Reactions in Clusters." His research interests are not only the spectroscopic study of reaction dynamics in hydrogen bonding clusters, recently, he strenuously studies conformational landscape of biomolecules in gas phase with developing new vaporization techniques.